



universität
wien

DIPLOMARBEIT

Titel der Diplomarbeit

Accelerator Mass Spectrometry of Cesium Isotopes

verfasst von

Magdalena Katharina Kasberger

angestrebter akademischer Grad

Magistra der Naturwissenschaften (Mag. rer. nat.)

Wien, 2015

Studienkennzahl lt. Studienblatt: A 190 412 406

Studienrichtung lt. Studienblatt: Lehramtsstudium UF Physik UF Mathematik

Betreut von: Univ.-Prof. Dipl.-Ing. Dr. Robin Golser

Abstract

Accelerator Mass Spectrometry (AMS) is a highly sensitive method to determine isotopic ratios in natural samples down to extremely low levels of about 10^{-15} . The challenge in measuring the cesium isotopes ^{135}Cs and ^{137}Cs is the isobaric interference of barium. Naturally occurring abundances are estimated to $^{135,137}\text{Cs}/^{133}\text{Cs} \approx 10^{-11}$. This thesis presents experiments on a possible separation of barium and cesium by extracting molecules from a negative ion source and injecting them into the accelerator, and tests on separation via different energy loss characteristics in the detector. Aside from these tests at the Vienna Environmental Research Accelerator (VERA), sufficient suppression should be achievable by the implementation of the Ion Laser InterAction Setup (ILIAS), utilizing the difference in the electron affinities of barium and cesium.

This preparatory study for AMS measurements of cesium isotopes includes tests on negative ion formation with sputtering by rubidium ions, on transmission and on detection. Stable Cs^- currents of several nA were extracted from the ion source. Comprehensive material tests included the investigation of cesium sulfate and cesium chloride regarding their performance in the ion source and the assessment of aluminum, copper, niobium and iron as matrix materials for the sputter targets. Furthermore, the effect of the incorporation of fluorides to the sample material was studied. The influences of type of stripper gas (He and Ar), stripper gas pressure and terminal voltage on the transmission through the accelerator of the created charge states were investigated. Transmissions of up to 28% in the 2+ charge state with argon stripping at 2.0 MV terminal voltage and up to 24% in the 3+ charge state with helium stripping at 2.9 MV have been achieved. Measurements were taken in two different ionization chambers at ion energies of 6–12 MeV and 26 MeV, respectively. On the whole, the present setup of VERA facilitates a detection limit in the region of $^{135,137}\text{Cs}/^{133}\text{Cs} \approx 10^{-9}$ with an overall efficiency of ca. 6×10^{-6} .

Zusammenfassung

Mit Nachweisgrenzen von bis zu 10^{-15} ist Beschleuniger-Massenspektrometrie (engl. Accelerator Mass Spectrometry, AMS) eine hochempfindliche Methode zur Bestimmung von Isotopenverhältnissen in natürlichen Proben. Die größte Herausforderung bei einer AMS Messung der Cäsium Isotope ^{135}Cs und ^{137}Cs ist die Unterdrückung ihrer Bariumisobare ^{135}Ba und ^{137}Ba . Es werden natürliche relative Isotopenhäufigkeiten im Bereich von $^{135,137}\text{Cs}/^{133}\text{Cs} \approx 10^{-11}$ erwartet. In dieser Diplomarbeit werden Untersuchungen zu einer möglichen Bariumunterdrückung in der Ionenquelle, sowie Tests bezüglich einer Trennung von Barium und Cäsium durch unterschiedlichen Energieverlust im Detektor vorgestellt. Unabhängig von diesen Ergebnissen am Vienna Environmental Research Accelerator (VERA) Labor, wird eine ausreichende Bariumunterdrückung durch die geplante Installation von ILIAS (Ion Laser InterAction Setup) durch Ausnutzen der unterschiedlichen Elektronenaffinitäten von Barium und Cäsium angestrebt.

Als eine vorbereitende Studie für zukünftige AMS Messungen von Cäsium Isotopen mit VERA, umfasst diese Diplomarbeit Experimente bezüglich negativer Ionenbildung durch Sputtering mit Rubidium Ionen, Transmission und Detektion. Es konnten stabile Cs^- Ströme von mehreren nA aus der Ionenquelle extrahiert werden. Als mögliche Target-Materialien wurden sowohl Cäsiumsulfat als auch Cäsiumchlorid in Bezug auf ihr Verhalten in der Ionenquelle umfassenden Tests unterzogen. Außerdem wurden Aluminium, Kupfer, Niob und Eisen auf ihre Eignung als Matrices geprüft. Der Effekt einer Beimischung eines Fluorids auf die negative Ionenbildung wurde ebenso untersucht. Es wurden umfangreiche Transmissionsmessungen durchgeführt, um den Einfluss von Art und Druck des Strippergases (He und Ar) sowie der Terminalspeisung auf die Transmission der einzelnen Ladungszustände zu bestimmen. Die besten Ergebnisse wurden in den Ladungszuständen 2+ mit bis zu 28% Transmission durch Argon Stripping bei 2.0 MV Terminalspeisung und im 3+ Ladungszustand mit bis zu 24% Transmission durch Helium Stripping bei 2.9 MV erreicht. Als Detektoren dienten zwei verschiedene Ionisationskammern, in denen mit Ionenenergien von 6–12 MeV und 26 MeV gemessen wurde. Insgesamt ermöglicht die derzeitige Ausstattung von VERA Nachweisgrenzen im Bereich von $^{135,137}\text{Cs}/^{133}\text{Cs} \approx 10^{-9}$ mit einer Gesamteffizienz von ca. 6×10^{-6} .

Contents

Abstract	i
Zusammenfassung	iii
1. Introduction	1
1.1. AMS of cesium	1
1.1.1. Applications and interest	1
1.1.2. Measurement: drawbacks and opportunities	1
1.2. The VERA facility	3
1.2.1. Cesium beam times at VERA	5
2. Negative ion source and injection	7
2.1. Rubidium sputtering of cesium	7
2.2. Negative ion formation	8
2.2.1. Material tests	8
2.3. Rubidium sputtering of typical AMS elements	13
2.4. Summary	15
3. Detection	17
3.1. Experiments on barium suppression via energy loss at VERA	17
3.1.1. Specific energy loss	17
3.1.2. Experimental setup	18
3.1.3. Evaluation and results	19
3.2. Setup with Bragg detector	22
3.2.1. m/q interferences	22
3.2.2. Standard and blank correction	23
4. Stripping process	27
4.1. Transmission in He and Ar	27
4.1.1. Experimental setup	27
4.1.2. Results	28
4.2. Charge state distribution in He and Ar	30
4.2.1. Experimental setup	32
4.2.2. Comparison with Sayer's model	32
5. Ratio measurements	37
5.1. Measured atomic ratios	37

Contents

5.2. Detection limit	43
5.3. Efficiency	45
5.4. Sequenced measurement	45
6. Conclusions and Outlook	49
Appendices	51
A. Potentials in chemical pretreatment	53
A.1. Precipitation of barium sulfate	53
Bibliography	57
Acknowledgments	61
Curriculum Vitae	63

1. Introduction

1.1. AMS of cesium

1.1.1. Applications and interest

Measuring ratios and concentrations of radioisotopes produced in anthropogenic fission is a successful method in environmental research. Especially the cesium isotope ^{137}Cs ($T_{1/2} = (30.08 \pm 0.09) \text{ a}$ (Browne and Tuli, 2007)) has proven to be a very useful time marker and tracer in oceanography (an overview was given by e.g. Aoyama and Hirose (2008)) and geology (for critical reviews see e.g. Parsons and Foster (2011) and Mabit et al. (2013)).

Nevertheless, the full potential of Cs isotopes can be exploited by also measuring the sister isotope ^{135}Cs with a half-life of $T_{1/2} = (2.3 \pm 0.3) \text{ Ma}$ (Singh et al., 2008). The combined measurement of ^{137}Cs and ^{135}Cs concentrations would provide much more information than ^{137}Cs as a tracer alone, as already emphasized by Lee et al. (1993). The ratio $^{135}\text{Cs}/^{137}\text{Cs}$ might be distinctive for the origin of production and just be a function of time, whereas the sole ^{137}Cs concentration could depend on e.g. sedimentation rate changes or physical/biological mixing of a sediment.

Assuming that a substantial amount of ^{135}Cs is produced by spontaneous fission of ^{238}U in the earth crust with a cumulative yield of 0.052 (England and Rider, 1993), the natural abundance of ^{135}Cs was estimated to be $^{135}\text{Cs}/^{133}\text{Cs} \approx 8 \times 10^{-12}$ by Lachner et al. (2015). However, strong fluctuations of its occurrence are to be expected, because of the high fractionation of uranium and cesium in minerals.

1.1.2. Measurement: drawbacks and opportunities

Due to its long half-life and the resulting low specific activity of environmental samples, decay counting of ^{135}Cs is impossible (Hou and Roos, 2008). Also, measuring $^{135,137}\text{Cs}/^{133}\text{Cs}$ ratios with mass spectrometry (MS) is difficult so far, as ^{135}Cs and ^{137}Cs both suffer from isobaric interference of the stable ^{135}Ba (relative isotopic abundance 6.59%) and ^{137}Ba (11.23%), respectively. Single approaches of MS techniques for determining atomic ratios of cesium isotopes have been made with e.g.

TIMS¹ (Delmore et al., 2011), RIMS² (Pibida et al., 2001) and ICP-MS³ (Granet et al., 2008). First results on cesium isotopic ratios using TIMS were accomplished by Lee et al. (1993) amounting to $^{135}\text{Cs}/^{133}\text{Cs} \approx 10^{-9}$ and $^{137}\text{Cs}/^{135}\text{Cs} \approx 0.5$ for coastal sediment samples associated to cesium coming from fallout. An analysis by Taylor et al. (2008), employing ICP-MS, presents ratios measured in sludge samples from a nuclear waste treatment pond ($^{135}\text{Cs}/^{137}\text{Cs} \approx 1$), soil samples from the Chernobyl exclusion zone ($^{135}\text{Cs}/^{137}\text{Cs} \approx 0.45$) and sediments collected downstream from a nuclear reactor with highly variable results. The strong variation of ratios suggest that $^{135}\text{Cs}/^{137}\text{Cs}$ alters with fuel and reactor conditions and therefore allows for identification of sources.

Furthermore, there have been first attempts on measuring cesium isotopic ratios with Accelerator Mass Spectrometry (AMS). In a negative ion source no full suppression of barium isobars can be achieved, since barium turned out to form stable negative ions (Kaiser et al., 1971) with an electron affinity of 0.14 eV (Petrinin et al., 1995). Though, Eliades et al. (2013) managed to suppress barium in the ion source down to $\text{BaF}_2^-/\text{CsF}_2^- \approx 5 \times 10^{-4}$ by injecting fluorides. Additionally, they have reported a possible reduction of barium in a NO_2 filled gas reaction cell down to ratios of $\text{BaF}_2^-/\text{CsF}_2^- \approx 2 \times 10^{-5}$. A combination of these methods suggests detection limits for cesium isotopic ratios of $^{135}\text{Cs}/^{133}\text{Cs} \approx 7 \times 10^{-15}$ and $^{137}\text{Cs}/^{133}\text{Cs} \approx 1 \times 10^{-14}$. Most recent achievements on this matter have been published by MacDonald et al. (2015), presenting a detection limit for $^{135}\text{Cs}/^{133}\text{Cs}$ of 1.3×10^{-10} . Results of the comprehensive study on accelerator mass spectrometry of cesium at VERA introduced in this thesis have partially been published by Lachner et al. (2015).

Chemical preparation

Isotopes of a certain element are characterized by identical proton number at different atomic mass. As the atomic number determines the electron shell structure, isotopes react similarly in chemical processes. (Nevertheless, some incomplete chemical reactions involving isotopes might suffer from fractionation effects.) Vice versa, in some cases, the chemical preparation of samples facilitates partial or full suppression of unwanted isobars. Often isobars feature completely different chemical characteristics utilized in target preparation. (Then different behavior in chemical reactions can be put to account e.g. by means of non synchronous precipitation of the compounds.)

¹Thermal Ionization Mass Spectrometry

²Resonance Ionization Mass Spectrometry

³Inductively Coupled Plasma Mass Spectrometry

1.2. The VERA facility

The Vienna Environmental Research Accelerator (VERA), a 3-MV Pelletron AMS facility, has been established in 1996 (Kutschera et al., 1997). Since then VERA has been upgraded and modified several times (e.g. Vockenhuber et al. (2003) or Priller et al. (2010)) — the present setup can be seen in Fig. 1.1. The main elements of the low-energy (LE) side before the accelerator are two MC-SNICS (Multi Cathode Source of Negative Ions by Cesium Sputtering) each providing space for 40 cathodes, two 45° electrostatic analyzers ($r = 0.300$ m) and the 90° injection magnet ($r = 0.457$ m) with a multi beam sequencer. The basic filtering components on the high-energy (HE) side are the analyzing magnet ($r = 1.270$ m) and another electrostatic analyzer ($r = 2.000$ m). For special purposes like heavy isotope detection (Steier et al., 2010), search for superheavy nuclides (Dellinger et al., 2011) or proton induced X-ray emission (PIXE) (Milota et al., 2008) a switching magnet leads to four additional beam lines.

So far, the layout of VERA facilitates the measurement of the most relevant AMS nuclides (for example ^{10}Be , ^{14}C , ^{26}Al , ^{36}Cl , ^{129}I , ^{236}U , ^{244}Pu) (Steier et al., 2004). VERA offers various ways of isobar suppression. Fortunately, some stable isobars do not form negative ions in the cesium sputter source (^{14}N , ^{26}Mg , ^{36}Ar , ^{129}Xe) and therefore, there is no demand for further effort in eliminating the isobaric background. Suppression of ^{10}B is achieved by utilizing the differences in energy loss of beryllium and boron in matter by placing a SiN-foil stack as an absorber before the detector (Schmidt, 2013). Furthermore, the installation of compact ionization chambers allowed for successful separation of ^{36}Cl and ^{36}S at ion energies of 24 MeV, which are possible with VERA's 3 MV accelerator (Martschini et al., 2013). Recently, isobar separation of ^{93}Zr and ^{93}Nb at 24 MeV was achieved with a new multi-anode ionization chamber (MAIC) (Martschini et al., 2015).

Moreover, VERA soon will be upgraded by ILIAS, the Ion Laser InterAction Setup, which is designed for performing laser photodetachment in an ion cooler (see Forstner et al. (2008) and Forstner et al. (2015)), a method for removing electrons from negative ions by excitation with laser radiation. Since Cs^- ($\text{EA} = 0.47164(6)$ eV) and Ba^- ($\text{EA} = 0.14462(6)$ eV) (see the review of Rienstra-Kiracofe et al. (2002)) have different electron affinities, this system is very promising to allow for sufficient Cs-Ba separation by employing an infrared laser with a photon energy between these two electron affinities. This method will significantly improve the detection limit of $^{135,137}\text{Cs}$.

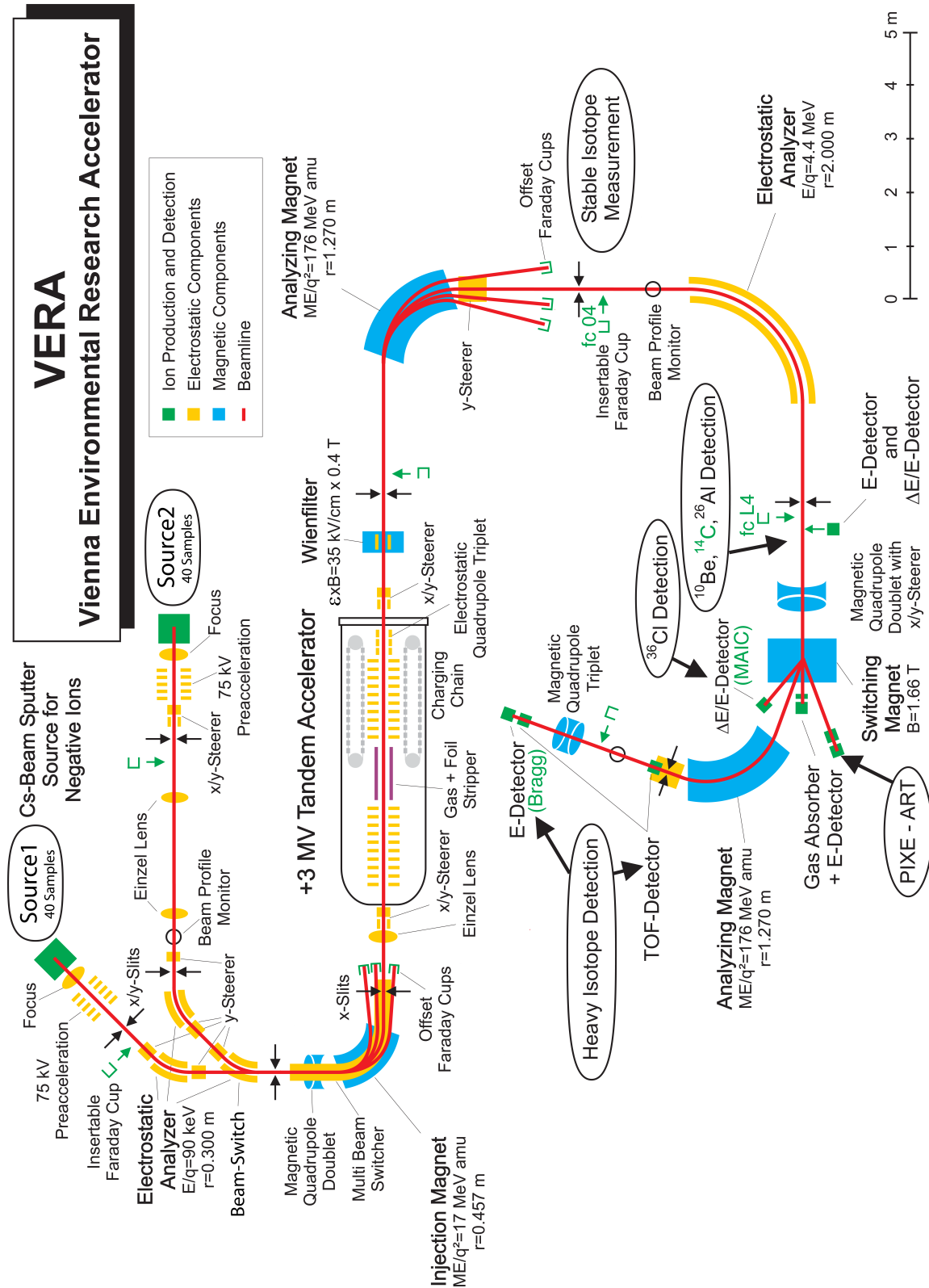


Figure 1.1.: The setup of the VERA AMS facility in May 2015.

1.2.1. Cesium beam times at VERA

In total, nine beam times (Cs1402, Cs1408, Cs1409, Cs1410, Cs1411, Cs1502, Cs1504, Cs1504b, Cs1504c) dealing with AMS measurements of cesium isotopes took place at VERA from February 2014 until May 2015. This thesis gives a summary of the major results. In each beam time, different aspects of an AMS measurement were emphasized:

name	ion source	detector	experiments
Cs1402	S2	MAIC	First tests on the barium suppression in an ionization chamber with split anodes (MAIC) via different energy loss.
Cs1408	S2	-	First tests on rubidium sputtering instead of cesium sputtering — negative ion formation of different materials; study on the transmission through the accelerator (especially concerning the charge state distribution and stripper gas pressure).
Cs1409	S2	Bragg	More material and transmission tests; first results on atomic ratios by taking measurements in a Bragg-type ionization chamber.
Cs1410	S2	Bragg	Assessment of rubidium sputtering by comparing the yields of major AMS elements; further measurements in the Bragg detector.
Cs1411	S2	Bragg	Further measurements in the Bragg detector. As reference: Optimization of ion source settings for C^- with rubidium sputtering.
Cs1502	S2	MAIC	Malfunction of the ion source and MAIC require maintenance; problems with the terminal voltage stability.
Cs1504	S1	MAIC	Final tests on the barium suppression in the MAIC detector.
Cs1504b	S2	Bragg	Development of a setup for a sequenced measurement of both, barium and cesium isotopes; taking first sequenced runs.
Cs1504c	S2	Bragg	Efficiency tests with weighted samples; more material tests in the Bragg detector.

2. Negative ion source and injection

The central component of the MC-SNICS at VERA (Priller et al., 2010) is a cooled sample wheel (holding up to 40 cathodes) placed opposite to the spherical ionizer (a hot surface of approx. 1000 °C) at a potential of -5 kV relative to the ionizer. The extractor is situated behind the ionizer and is kept at an average potential of -15 kV. In sum, the whole source lies at a potential of -70 kV (-5 kV cathode voltage, -15 kV extraction voltage plus -50 kV source voltage). Metallic cesium is used for sputtering the samples. A cesium reservoir is surrounded by an oven, which is heated to temperatures of about 150 °C. Cesium vaporizes into the space between ionizer and sample wheel. The cesium vapor will both ionize to Cs^+ on the hot ionizer surface and condense on the wheel. The positive cesium ions are accelerated to the cathode and sputter target particles through the condensed cesium layer. Due to its low electron affinity, cesium donates electrons to the sputtered sample atoms, which then form negative ions or molecules (Middleton, 1983). As the total acceleration voltage adds up, a total ion energy of 70 keV is reached.

The source output is mainly regulated by the amount of cesium transferred into the source. Increasing the temperature of the Cs-oven and the „line heater,, (i.e. the capillary connecting the cesium reservoir with the source) will enhance the cesium influx into the source. Further, a higher temperature of the ionizer will increase the rate of ionized cesium atoms and thus lead to a higher output of the source.

The pre-accelerated particles then have to pass a number of consecutive filters on the low-energy side. First the electrostatic analyzer (ESA) selects for particles of the same energy-over-charge ratio (E/q). After the ESA, the ion beam is monoenergetic, since ions and molecules extracted from the source are in charge state -1. The first separation of masses is achieved in the injection magnet, where particles with same magnetic rigidity (mv/q) follow the same trajectories. VERA’s injector is equipped with a multi beam sequencer, a mechanism to accelerate and decelerate the ion beam by up to 12 keV. It allows to sequentially inject different masses into the accelerator without changing the magnetic field.

2.1. Rubidium sputtering of cesium

As conventional cesium sputtering would distort the $^{135}\text{Cs}/^{133}\text{Cs}$ ratio of a sample, rubidium was tested as sputter material. Both, cesium and rubidium, belong to the

CHAPTER 2. Negative ion source and injection

first main-group of the periodic table and therefore they have very similar chemical properties. In Table 2.1 a comparison of some relevant characteristics of cesium and rubidium is given.

Table 2.1.: Properties of rubidium and cesium. Electronegativity EN is given in the Pauling scale. For comparison: In the periodic table of elements francium has the lowest and fluorine the highest electronegativity with $EN(\text{Fr})=0.7$ and $EN(\text{F})=3.98$, respectively.

element	atomic number	stable isotopes	melting point	boiling point	EN
rubidium	37	^{85}Rb (72.17%) ^{87}Rb (27.83%)	39.30 °C	688 °C	0.82
cesium	55	^{133}Cs (100%)	28.5 °C	671 °C	0.79

As both of VERA's ion sources usually are equipped with cesium, source S2 had to be opened and provided with rubidium for each beam time. In the course of these reservoir changes, the source was not cleaned each time. Therefore, impurities arising from cesium residues are to be expected. Especially at high ionizer settings, accumulated cesium on the hot ionizer surface might be released due to a cleaning effect. In beam time Cs1410 the rubidium reservoir was empty, but sputtering still was possible at a high ionizer power, which indicates the cleaning effect.

In summary, rubidium is suited for the use as sputter material in an ion source. Detailed characteristics like source settings, negative ion formation on different sample materials and intensity of current for both, cesium and several typical AMS elements, are presented in the following sections.

2.2. Negative ion formation

2.2.1. Material tests

For all tests a copper wheel along with aluminum and copper cathodes were used.

Selection of cesium compound as target material

As cesium is an alkali metal, it is highly reactive in its elemental form. So there is a need for a preferably non hazardous compound, which allows for efficient negative ion formation in the ion source. Also, a high melting point and good thermal and electric conductivity are eligible in the ion source (Middleton, 1983). Because of its high melting point of 1006 °C, cesium sulfate (Cs_2SO_4) was supposed to be the

2.2. Negative ion formation

most promising cesium compound. As an alternative, cesium chloride (CsCl) with a lower melting point at $646\text{ }^{\circ}\text{C}$ was tested.

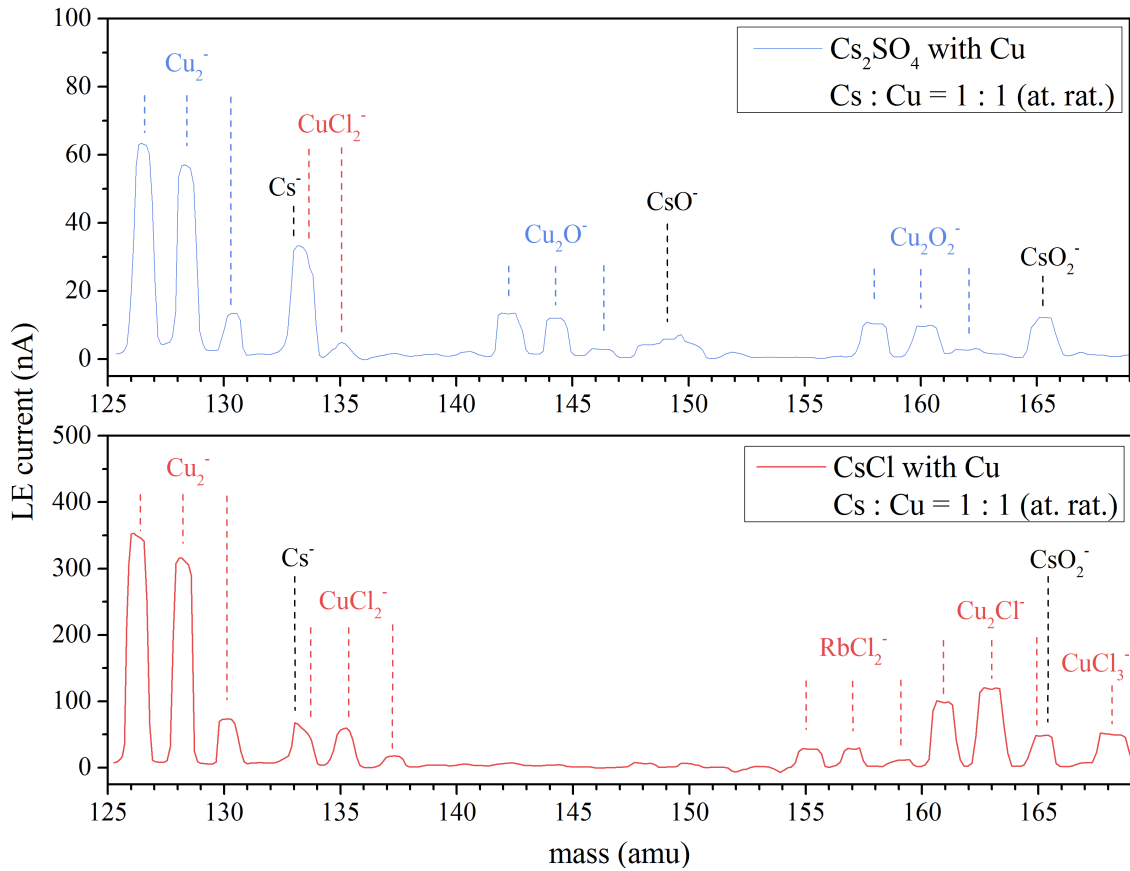


Figure 2.1.: Mass scans on a cesium sulfate and a cesium chloride sample, respectively, each mixed with copper at an atomic ratio of $\text{Cs}:\text{Cu} = 1:1$. The dashed lines denote the position of isotopologues (i.e. molecules that only vary in their isotopic composition) of molecules indicated in the plot. (Measured in Cs1408 .)

In order to find out which molecules are formed in the ion source, the mass spectra of both Cs_2SO_4 and CsCl were recorded. In Fig. 2.1 mass scans of cesium sulfate and cesium chloride targets are shown, respectively. Such mass scans were performed by gradually altering the magnetic field of the injection magnet while measuring the current in the Faraday cup in front of the accelerator (see Fig. 1.1). As the injection magnet's Hall probe does not read the value of the magnetic field accurately, the mass scans possess a linear offset. Distinctive peaks, e.g. Cu_2^- , were used as calibration points to shift the peaks to correct mass positions.

Peaks at masses 133, 149 and 165 can be assigned to the cesium compounds Cs^- , CsO^- and CsO_2^- , respectively. Both spectra in Fig. 2.1 show peaks at mass 135. It is well known that spectra of samples containing aluminum show a peak of the molecular ion Al_5^- ($m = 135$ amu) (Middleton, 1989). Since aluminum was neither used for cathode or sample in the present mass spectra, the peak might stem

from CuCl_2^- . Unfortunately, cesium chloride seems to vaporize in the ion source and leads to contaminations on several cathodes of the target wheel, as the peak also occurred on cathodes not containing chlorine. Those disturbing molecular mass interferences (the mass spectrum of CuCl_2 consists of masses 133, 135, 137 and 139 amu) are observed on most spectra recorded in that beam time. Such suspected molecular interferences complicate measurements, as it is unclear what molecules or ions constitute the particle current during tuning processes. Based on relative abundances of the chlorine isotopes ^{35}Cl (75.8%) and ^{37}Cl (24.2%), the $^{133}\text{Cs}^-$ fraction of the current measured on 133 amu can be estimated. In the cesium sulfate spectrum shown in Fig. 2.1, the Cs^- fraction of the peak at mass 133 is 88%, but in other measurements the ratio drops to 51%. These circumstances rule out the use of cesium chloride as suitable sample material in combination with a copper wheel and copper cathodes for cesium measurements.

Comparing the currents of Cs^- , CsO^- and CsO_2^- suggests Cs^- as the most intense negative ion for injection. For example is $\text{Cs}^-/\text{CsO}_2^- \approx 3$ (already corrected for the chlorine fraction) in the cesium sulfate spectrum shown in Fig. 2.1. Though oxides yielded particularly high currents on pure cesium sulfate samples, mass scans on barium samples show that barium forms oxides even better (see section below). Sputtering cesium sulfate yielded a up to 60 nA stable Cs^- current on the low-energy side. Fig. 2.2 exemplarily shows the time development of the Cs^{2+} current at usual settings used for measurements. The current increases with time from approximately 2.3 nA to 3.3 nA on the high-energy side and shows no significant fluctuations. Hence, rubidium sputtering of cesium sulfate is satisfactory in terms of intensity and stability of the current. (For another example of temporal current development, see Fig. 5.6.)

Tests on barium reduction

Experiments on possible barium suppression have also been conducted by injecting CsF_2^- (or if applicable other fluorides), since reduction factors of $\text{BaF}_2^-/\text{CsF}_2^- \approx 5 \times 10^{-4}$ for the negative ion production in the ion source have been reported by Eliades et al. (2013). To introduce fluorine into the source, powdered lanthanum(III) fluoride (LaF_3) and lead(II) fluoride (PbF_2) have been employed as mixing materials. In the tests referred in Eliades et al. (2013), PbF_2 was used as matrix, but LaF_3 is preferable concerning safety as it is non carcinogen. Samples containing cesium sulfate (Cs_2SO_4), barium sulfate (BaSO_4) and one of the mentioned fluorides have been prepared at atomic ratios of $\text{Cs}:\text{Ba}:\text{F} = 1:1:8$.

Mass scans of the described samples are shown in Fig. 2.3. According to the scans, both, LaF_3 and PbF_2 , suppress the formation of Cs^- in the ion source. As anticipated, the dominant cesium molecule is CsF_2^- instead (e.g. 14 nA on the lead(II) fluoride target). The average reduction factor of some intermittent measurements

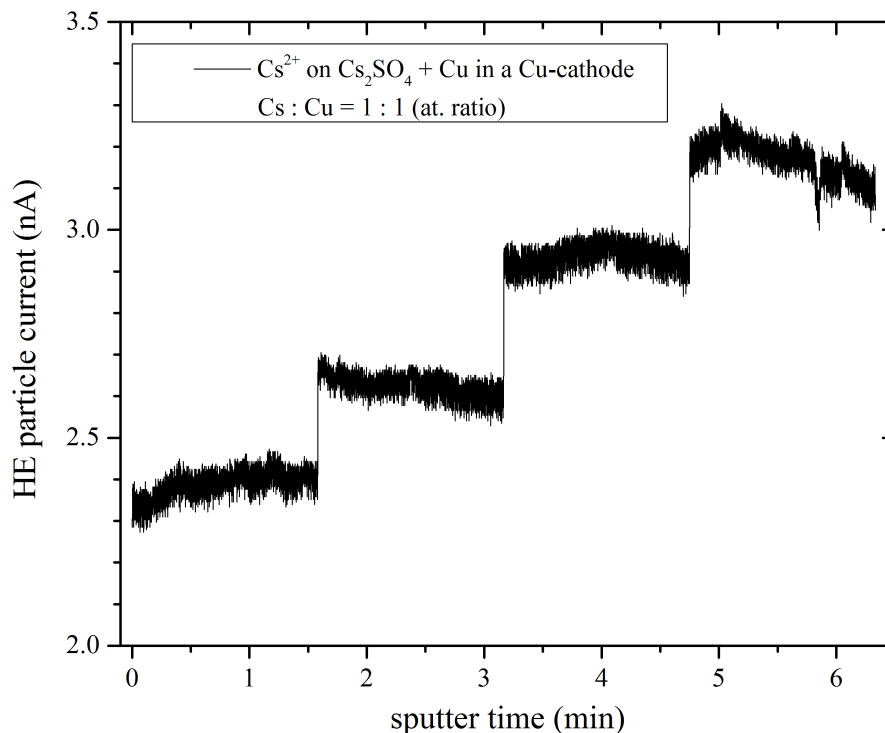


Figure 2.2.: High-energy current vs. sputter time during a measurement on a copper-mixed cesium sulfate sample (Cs:Cu = 1:1 atomic ratio) in a copper cathode at 1.6 MV terminal voltage in the 2+ charge state. The current is normed by the charge state of the particles. The scattering during a run dominates the periodicity of the current with a frequency of the cycle duration (95 ms). The four sections correspond to consecutive runs of a measurement. (Cs1409)

is $\text{BaF}_2^-/\text{CsF}_2^- = (8 \pm 3) \times 10^{-2}$ (see also Table 2.3). The great disadvantage of injecting fluorides was the instability of currents.

Some peaks, especially in the vicinity of 195 amu, could not be assigned unambiguously. The molecules labeled in Fig. 2.3 may contribute, but the relative heights of the peaks suggest contributions of unknown origin.

To further examine the relative negative ion yields for cesium and barium molecules, an aluminum cathode was filled with cesium sulfate, barium sulfate and copper (Cs:Ba:Cu = 1:1:3 atomic ratio). Mass scans on this target show an enhanced output of barium oxides (Fig. 2.4). Average suppression of barium molecules in several mass scans on this target could be calculated to $\text{Ba}^-/\text{Cs}^- = 0.4 \pm 0.1$, $\text{BaO}^-/\text{CsO}^- = 4.3 \pm 1.1$ and $\text{BaO}_2^-/\text{CsO}_2^- = 1.5 \pm 0.3$, respectively (see also Table 2.3). For the reduction factors, currents assigned to ^{138}Ba molecules were divided by the relative isotopic abundance of ^{138}Ba (71.1%). This provides comparability

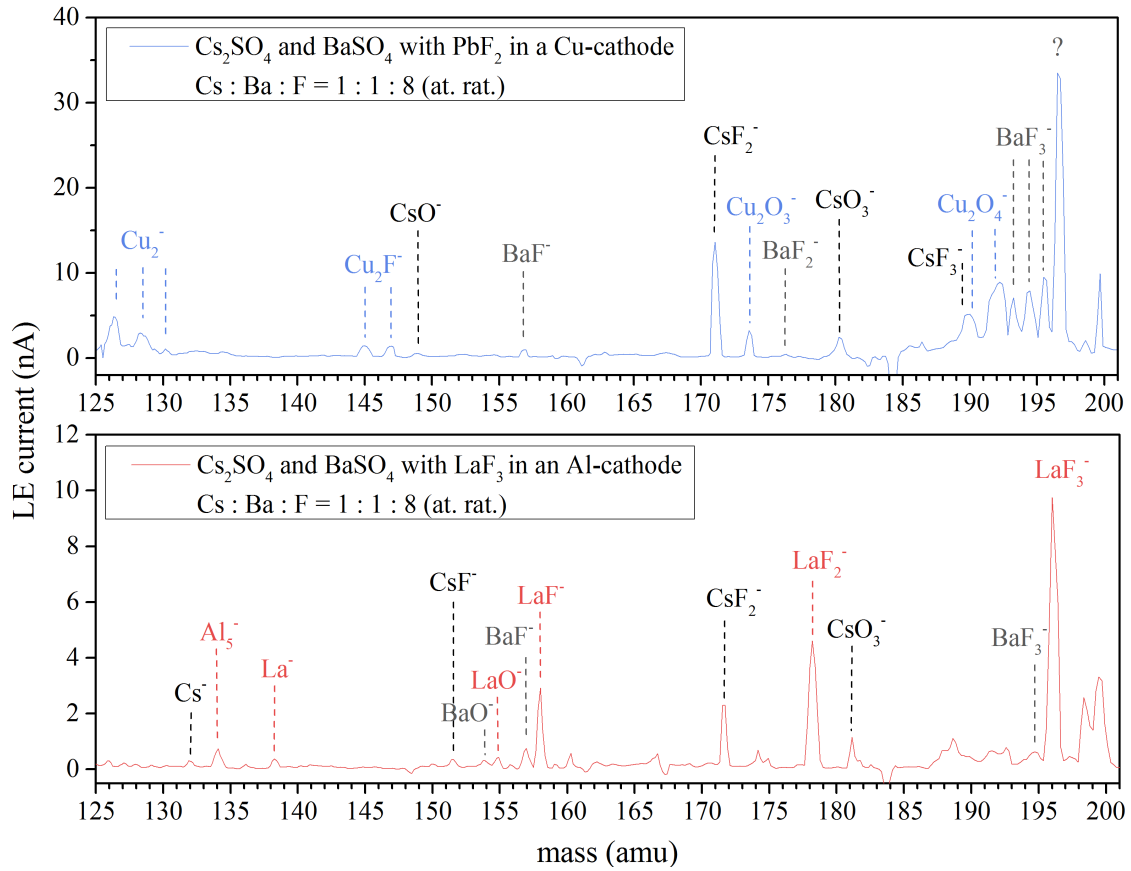


Figure 2.3.: This figure shows mass scans on cesium sulfate and barium sulfate mixed with lead(II) fluoride or lanthanum(III) fluoride, respectively. The calibration in the second plot is not very accurate for lower masses. Whenever possible, intense peaks were identified — the origin of the peak at mass 196 amu might be $^{138}\text{BaF}_3\text{H}^-$, as barium forms hydrides well (Middleton, 1989). (Measured in Cs1409.)

with cesium currents regarding negative ion formation in the source, as ^{133}Cs has a relative isotopic abundance of 100%.

Matrix material test

Metallic matrices may have a positive effect on negative ion formation, as they improve electrical and heat conductivity in the sample. Furthermore, especially when handling small sample sizes, it can be useful to mix the sample of interest with other materials. Also, sputter times can be extended by mixing the sample. Thus, cesium sulfate has been mixed with iron, copper and niobium at different atomic ratios. The mass spectra of iron and niobium mixtures (see lower spectrum in Fig. 2.5) both show little Cs^- output. The niobium spectra are dominated by niobium oxides (NbO_x , several hundreds of nA) and show unidentified peaks at

2.3. Rubidium sputtering of typical AMS elements

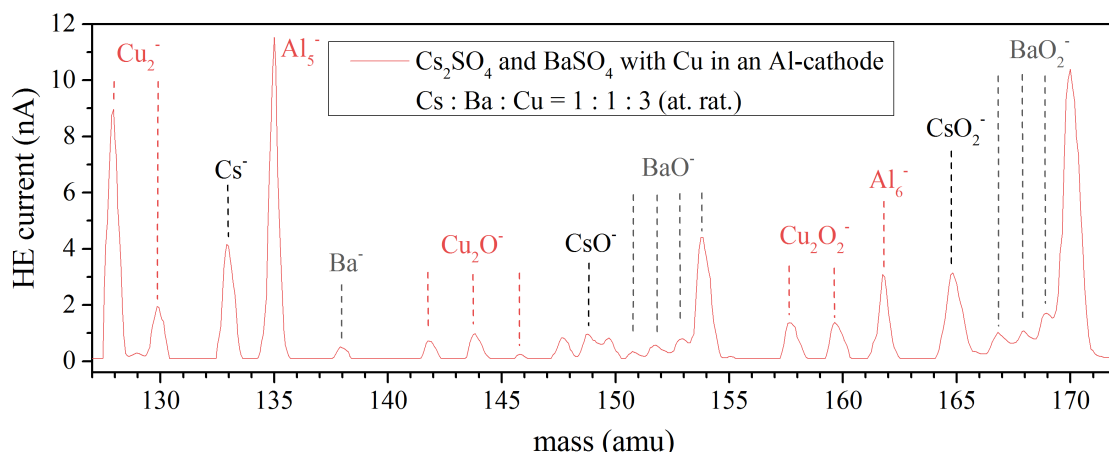


Figure 2.4.: Mass scan on cesium sulfate and barium sulfate mixed with copper. (Measured in Cs1408.)

masses 132 and 147 amu. Iron mixtures form oxides (Fe_2O_x) as well, but not as intense as niobium. After a sputtering time of about 15 minutes, iron and niobium mixtures yielded LE currents not exceeding 4 nA Cs^- .

In principle, the addition of copper does not alter the spectrum of pure cesium sulfate (see upper spectrum in Fig. 2.5). Whereas pure cesium sulfate resulted in 15 nA Cs^- , Cs:Cu=1:1 yielded approximately 10 nA Cs^- at the same ion source settings (also sputtered for 15 minutes). Further dilution with copper reduced the Cs^- current, though not proportionally — average LE Cs^- currents of 5 nA and 2.5 nA were produced for Cs:Cu=1:3 and Cs:Cu=1:10, respectively.

2.3. Rubidium sputtering of typical AMS elements

In order to obtain a comprehensive comparison of cesium and rubidium sputtering, the LE currents of a selection of well known AMS elements yielded with rubidium sputtering were studied. For each element, two cathodes were sputtered for up to 15 minutes at usual source settings for the respective element. Average currents obtained at the end of this time are listed in Table 2.2. Optimizing the source output was merely attempted for carbon. By slightly increasing the temperature of the Rb-oven, the line heater and the ionizer compared to usual settings a current of 20 μA C^- was obtained. Generally, yields for negative ion formation with rubidium sputtering are similar as for cesium sputtering and therefore sufficiently high for the use of AMS measurements.

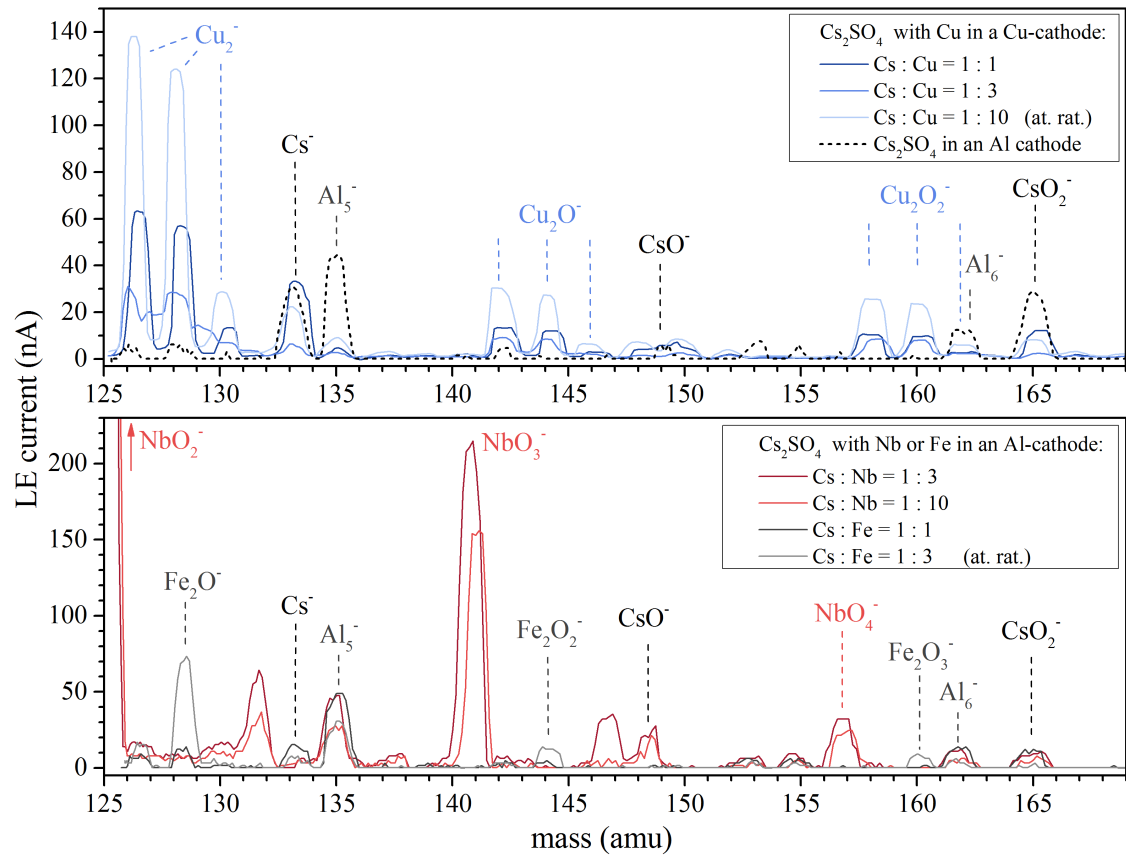


Figure 2.5.: Mass spectra of cesium sulfate mixed with metals (Fe, Cu, Nb) at different mixing ratios. (Measured in Cs1408.)

Table 2.2.: Comparison of various AMS elements frequently measured at VERA regarding the LE currents achieved via rubidium and cesium sputtering, respectively.

element	inj. molecule	material	(Rb)	(Cs)
C	$^{12}\text{C}^-$	graphite	17 μA	15–30 μA
Be	$^9\text{Be}^{16}\text{O}^-$	beryllium(II) monoxide, copper	800 nA	1–1.5 μA
F	$^{19}\text{F}^-$	lithium fluoride	650 nA*	650 nA*
Al	$^{27}\text{Al}^-$	aluminum(III) oxide, copper 4:1 vol. mixture	100 nA	80–120 nA
Cl	$^{35}\text{Cl}^-$	silver chloride	6 μA	5–6 μA
Cs	$^{133}\text{Cs}^-$	cesium sulfate, copper 1:1 at. mixture	10 nA	-

* $^{19}\text{F}^-$ currents can be easily enhanced by turning up temperatures in the ion source for both, Rb and Cs sputtering.

2.4. Summary

Altogether, rubidium sputtering in combination with cesium sulfate as sample material (if required mixed with copper) seems to make the AMS measurements of ^{135}Cs feasible. Injecting Cs^- yielded best results regarding intensity and durability of the LE current. However, further suppression of barium will be necessary, as $\text{Ba}^-/\text{Cs}^- = 0.4 \pm 0.1$ was the average reduction accomplished in the ion source. This value needs to be improved by orders of magnitude. An overview of the achieved barium reduction in the ion source for the most important molecules is given in Table 2.3.

Table 2.3.: Reduction of the barium background in the ion source by injecting different molecules. Currents used for calculation of the ratios were measured in the Faraday cup right after the injection magnet (Cs1409).

molecules formed in the ion source	reduction ratio
Ba^-/Cs^-	0.4 ± 0.1
$\text{BaO}^-/\text{CsO}^-$	4.3 ± 1.1
$\text{BaO}_2^-/\text{CsO}_2^-$	1.5 ± 0.3
$\text{BaF}_2^-/\text{CsF}_2^-$	$(8 \pm 3) \times 10^{-2}$

3. Detection

Only a couple of nuclides can be separated from their unwanted isobars (i.e. nuclides with nearly identical mass) by conventional AMS (e.g. ^{10}Be , ^{36}Cl , ^{41}Ca , ^{53}Mn , ^{60}Fe , ^{63}Ni). However, as a „gift of nature“, some of these isobaric interferences do not affect AMS measurements (e.g. the fact that ^{14}N does not form negative ions is beneficial in ^{14}C measurements). Unfortunately, in case of ^{135}Cs and ^{137}Cs , both nuclides suffer from interferences by their only stable isobars ^{135}Ba (relative isotopic abundance 6.59%) and ^{137}Ba (11.23%), respectively. Thus, detected events of masses 135 amu or 137 amu in chemically purified and natural samples (generally not contaminated) have to be assigned to barium. As a consequence, suppression of the barium background is crucial and was tried to be achieved through the detection setup. Though no sufficient separation was reached, measuring the atomic ratios $^{135,137}\text{Ba}/^{133}\text{Cs}$ of both, cesium and blank samples, at least gives an estimate of the purity of the used materials, partial isobar suppression in various steps of the measuring procedure and the detection limit of the setup, respectively.

3.1. Experiments on barium suppression via energy loss at VERA

An attempt to reduce the barium background was by means of a potential difference in energy loss characteristics. In the MAIC detector (see section 3.1.2) behind the switching magnet successful separations of isobar systems at 60 amu and 93 amu have already been achieved (Martschini et al., 2015).

In order to get an idea of the possible behavior of ^{135}Cs and ^{135}Ba in the detector, a count rate of the unstable nuclide ^{133}Ba was simulated by injecting the isotopes $^{132,134,135}\text{Ba}^{8+}$ at the same magnetic rigidity as $^{133}\text{Cs}^{8+}$ into the MAIC detector. Comparison of the individual energy losses of the different ion species may reveal mass and atomic number dependencies.

3.1.1. Specific energy loss

The main interaction of ions penetrating matter is due to Coulomb forces between those ions and the shell electrons belonging to the absorber atoms. Depending on the

ion's energy E , the interaction results either in excitation of an electron within the absorber atom (i.e. lifting it to a higher shell) or in ionizing the atom by detaching an electron. Since the maximum energy that can be transmitted from the ion (m, E) to an electron m_e , is only $4Em_e/m$, many interactions with the absorber are necessary to fully stop the primary particle. At low energies nuclear stopping (i.e. elastic collisions with the nuclei in the absorber material) contributes, too. Further, the probability for nuclear stopping increases with the projectile mass.

The linear stopping power or specific energy loss S is defined as the differential energy loss per differential path length:

$$S = -\frac{dE}{dx} \quad (3.1)$$

S depends on the velocity v and the squared charge $(ze)^2$ of the incident ion, the number density N and the atomic number Z of the absorber atoms and can be calculated by the Bethe formula:

$$-\frac{dE}{dx} = \frac{4\pi e^4 z^2}{m_e v^2} N B \quad (3.2)$$

where

$$B = Z \left[\ln \frac{2m_e v^2}{I} - \ln \left(1 - \frac{v^2}{c^2} \right) - \frac{v^2}{c^2} \right]$$

I is an experimental parameter that denotes the average excitation and ionization potential of the absorber (e.g. $I = 10.74$ eV for isobutane). The atomic numbers Z and z may be replaced by the effective atomic numbers Z_{eff} for molecular gases (e.g. $Z_{eff} \approx 5.33$ for isobutane C_4H_{10}) and z_{eff} for the projectile, as the Bethe formula describes the electronic stopping of fully stripped projectiles. (Knoll, 1989, p. 31 ff)

Since S is proportional to the square of the projectiles atomic number z , different energy loss in the detector material (e.g. the counting gas within an ionization chamber) for isobaric systems of sufficient high $\Delta z/z$ provides an opportunity for separation of isobars.

3.1.2. Experimental setup

MAIC detector

The Multi Anode Ionization Chamber (MAIC) is a novel, gas filled ionization chamber with three split anodes A1, A2 and A3 engineered at VERA (Buchriegler, 2013).

3.1. Experiments on barium suppression via energy loss at VERA

It is equipped with a Frisch grid and an aperture between anodes A2 and A3. Isobutane is used as counting gas at variable pressures. The detector is mounted at the end of the +40°-beamline as plotted in Fig. 1.1, where it is labelled as $\Delta E/E$ -Detector (MAIC).

Machine setup and measurement

Negative ions were formed and extracted out of ion source S1 by cesium sputtering. A Cs^- current was attained by sputtering blank copper cathodes, as sputtering metals with cesium is known to enhance the Cs^- output (Middleton, 1989). Barium was injected as Ba^- from barium carbonate. To reach high energies while still ensuring acceptable transmission through the accelerator, the machine is tuned for the 8+ charge state. Oxygen was used as stripper gas in the accelerator at 2.85 MV terminal voltage. If necessary, the beam was attenuated via a grid by factors of 100, 300 or 30000. Without attenuation, the intensity of mass 132 was approximately 2.5×10^4 events/s, 2.5×10^6 events/s for mass 133, 6×10^4 events/s for mass 134 and the intensity of mass 135 was 6×10^4 events/s on anode A3, respectively. To vary the number density N of the detector gas and check for full stopping of the injected nuclides, the measurement was conducted both, at 28 mbar and 33 mbar gas pressure, in the ionization chamber for masses 132, 133, 134 and 135 amu. Measurements were performed in 1000 to 6000 cycles (each 95 ms) at an approximate count rate of 100 events/s.

3.1.3. Evaluation and results

The tests have shown that separation of barium and cesium in the detector is no prospect at an ion energy of 25.8 MeV. In vera2 (the data evaluation system of VERA) the barycenters of the $^{132,134}\text{Ba}$ events were computed with the „FIND _ PEAK _ SHIFT“ evaluation and shifted to their common average for every anode, marking the hypothetical ^{133}Ba . The barycenters of $^{132,134,135}\text{Ba}$ events, respectively, show linear dependency (see Fig. 3.1). The values of the original and shifted peaks are listed in Table 3.1. In Fig. 3.2 and Fig. 3.3 the simulated energy loss of ^{133}Ba (on anode A3 compared to anodes A1+A2) is quite the same as for ^{133}Cs . Similar results are gained by plotting the energy loss on A1 vs. A3 and A2 vs. A3. Therefore a distinction of cesium and barium isobars in the detector appears to be unfeasible at VERA (cf. (Martschini et al., 2015) for an example of successful separation in the detector). The particles were already fully stopped in the detector at 33 mbar gas pressure (in Fig. 3.3 all events nearly lie on one line), therefore further investigations at higher gas pressures are not necessary.

CHAPTER 3. Detection

Table 3.1.: The barycenters of events on anodes A1, A2 and A3 for different gas pressures in the ionization chamber. $^{133}\text{Ba}^{8+}$ (sim.) denotes the simulated peak, calculated as the linear interpolation between $^{132}\text{Ba}^{8+}$ and $^{134}\text{Ba}^{8+}$.

Anode	A ₁	A ₂	A ₃
28 mbar			
$^{132}\text{Ba}^{8+}$	2086.92 ± 0.53	1356.04 ± 0.38	789.38 ± 0.16
$^{133}\text{Cs}^{8+}$	2057.63 ± 0.90	1355.47 ± 0.01	785.8 ± 1.1
$^{133}\text{Ba}^{8+}$ (sim.)	2059.78 ± 0.27	1346.53 ± 0.66	787.82 ± 0.55
$^{134}\text{Ba}^{8+}$	2032.20 ± 0.67	1335 ± 1	787.46 ± 0.98
$^{135}\text{Ba}^{8+}$	2005.80 ± 0.23	1327.76 ± 0.07	783.6 ± 1.2
33 mbar			
$^{132}\text{Ba}^{8+}$	2360.31 ± 0.20	1411.1 ± 1.6	684.31 ± 0.58
$^{133}\text{Cs}^{8+}$	2328.3 ± 1.1	1406.7 ± 1.4	680.97 ± 0.38
$^{133}\text{Ba}^{8+}$ (sim.)	2330.42 ± 0.12	1404.2 ± 1.3	683.83 ± 0.47
$^{134}\text{Ba}^{8+}$	2300.43 ± 0.24	1395.78 ± 0.03	682.0 ± 1.3
$^{135}\text{Ba}^{8+}$	2271.08 ± 0.47	1385.1 ± 1.4	683.19 ± 0.35

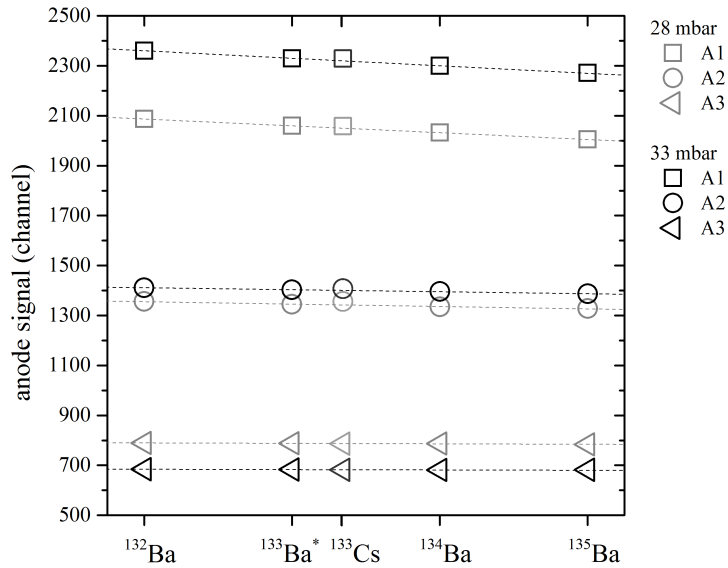


Figure 3.1.: Channel barycenters of the detected $^{132,134,135}\text{Ba}$ and ^{133}Cs events on anodes A1, A2 and A3 at gas pressures of 28 and 33 mbar, respectively. “ $^{133}\text{Ba}^*$ ” denotes the average of the $^{132,134}\text{Ba}$ peaks. The dashed line represents the linear regression through the points at 132 amu and 134 amu for each anode and pressure — Pearson’s r is < -0.99 , i.e. nearly total negative correlation. Error bars are smaller than the size of the icons. (Measurements were taken in Cs1504.)

3.1. Experiments on barium suppression via energy loss at VERA

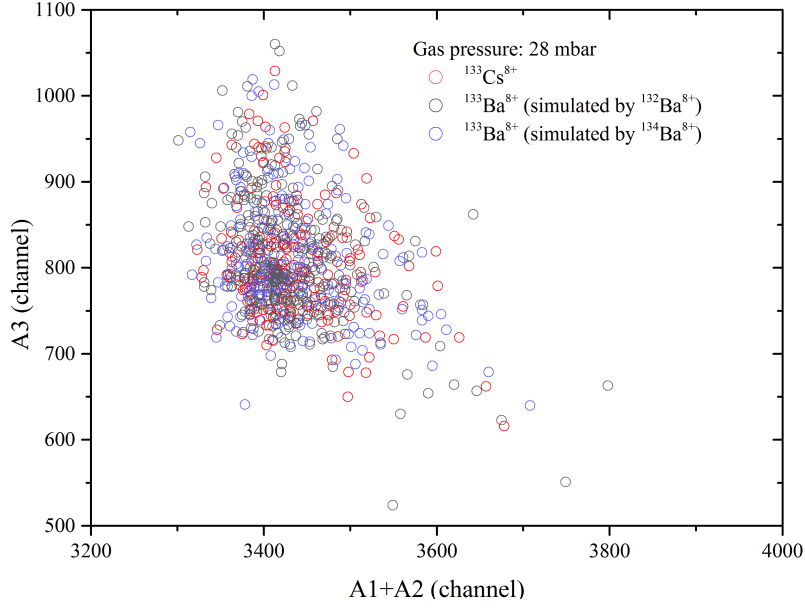


Figure 3.2.: Uncalibrated energy loss of the injected ions detected at anode A3 plotted vs. the energy loss detected at anodes A1 and A2 at the MAIC detector at 28 mbar gas pressure. Whereas $^{133}\text{Cs}^{8+}$ (from blank copper cathodes) was injected into the detector, hypothetical $^{133}\text{Ba}^{8+}$ counts were simulated by injecting $^{132}\text{Ba}^{8+}$ and $^{134}\text{Ba}^{8+}$ (all of the same magnetic rigidity) from barium carbonate samples, respectively. The plot only shows every 75th event. (Measured in Cs1504.)

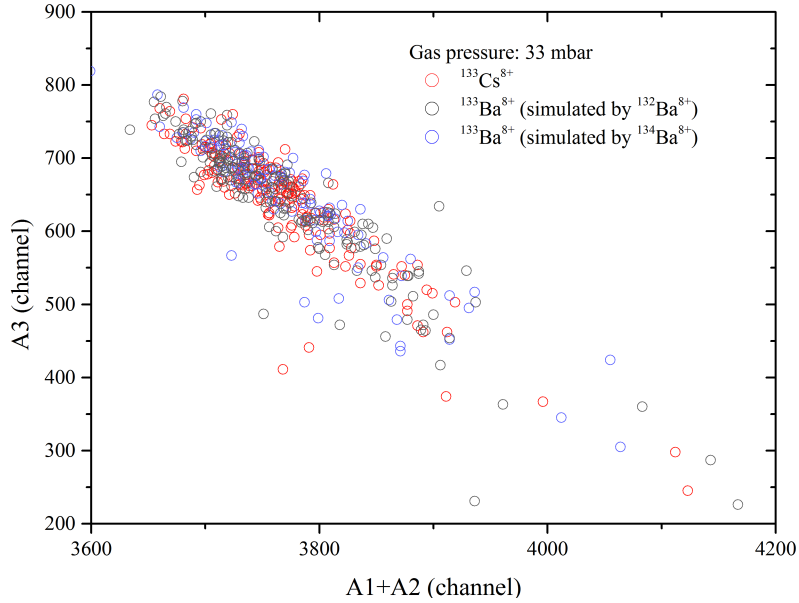


Figure 3.3.: Energy loss of ^{133}Cs from blank copper cathodes and simulated ^{133}Ba events from barium carbonate samples at anode A3 vs. the energy loss at anodes A1 and A2 in MAIC at 33 mbar gas pressure. The plot only shows every 75th event. (Measurements were taken in Cs1504.)

3.2. Setup with Bragg detector

Since high energies (hence also high charge states) do not entail any benefit in $\Delta z/z$ separation in the detector, efforts were made in finding a measurement setup providing highest possible transmission through the accelerator. In several beam times, different stripper gases (He, Ar, O₂), stripper gas pressures and terminal voltages were tested in order to improve the transmission. Furthermore the charge state distribution after the accelerator was studied by using a Wien filter. The results of these investigations are described in chapter 4 in more detail. Nevertheless the resulting magnetic rigidity at energies ranging from ≈ 6 MeV to 12 MeV is too high to reach the MAIC detector in the +40°-beamline by means of the installed switching magnet. Some measurements were taken with so called “shorting rods” applied to the accelerator. These are metallic rods to shorten the accelerator tubes in order to improve ion optics for terminal voltages < 2 MV.

On this account the Bragg detector, mounted at the end of the +20°-beamline, was used for most further measurements. It is an ionization chamber with a 5×5 mm² SiN window (two different thicknesses were used: 50 nm and 1000 nm) operated at 30 mbar isobutane gas pressure. The detector is operated at an anode potential of 850 V and a Frisch grid voltage of 450 V.

3.2.1. m/q interferences

Ions run through several filtering processes when being analyzed with AMS. The main components are electrostatic analyzers and bending magnets, which sort out for energy over charge \mathcal{E}/q and momentum over charge $\sqrt{2m\mathcal{E}}/q$, respectively. Considering (molecular) ions which are injected with mass M and analyzed for $(m_i, q_i, \mathcal{E}_i)$, equations 3.3 and 3.4 show that ions (m, q, \mathcal{E}) with same mass over charge fraction also pass the high energy side filters. Thus, choosing the charge state for the measurement setup requires some thoughts, as a non integer mass over charge fraction for the isotope of interest can prevent such interferences.

$$\begin{aligned} \frac{\mathcal{E}}{q} &= \frac{m}{qM} (U_{\text{source}} + U_{\text{terminal}}) + U_{\text{terminal}} = \\ &= \frac{m_i}{(\frac{m_i}{q_i} = \frac{m}{q}) q_i M} (U_{\text{source}} + U_{\text{terminal}}) + U_{\text{terminal}} = \frac{\mathcal{E}_i}{q_i} \end{aligned} \quad (3.3)$$

$$\begin{aligned} \frac{\sqrt{2m\mathcal{E}}}{q} &= \sqrt{2 \left(\frac{m^2}{q^2 M} (U_{\text{source}} + U_{\text{terminal}}) + \frac{m}{q} U_{\text{terminal}} \right)} = \\ &= \sqrt{2 \left(\frac{m_i^2}{q_i^2 M} (U_{\text{source}} + U_{\text{terminal}}) + \frac{m_i}{q_i} U_{\text{terminal}} \right)} = \frac{\sqrt{2m_i\mathcal{E}_i}}{q_i} \end{aligned} \quad (3.4)$$

Interferences with cesium

Concerning the cesium measurements, the nuclides of interest are $^{135,137}\text{Cs}$ and ^{138}Ba (for a possible background correction, see section 5.4). Regarding yield and transmission, the most favorable charge states are 2+ and 3+ as described in chapter 4. These charge states might show m/q interferences (Table 3.2).

Table 3.2.: m/q interferences with cesium und barium isotopes in 2+ and 3+ charge states.

m/q interferences	charge state [e]	stable isotope	at. number	abundance [%]
$^{135}\text{Cs}^{3+}$	1+	^{45}Sc	21	100
	2+	^{90}Zr	40	51.45
	3+	^{135}Ba	56	6.592
$^{138}\text{Ba}^{2+}$	1+	^{69}Ga	31	60.108
$^{138}\text{Ba}^{3+}$	1+	^{46}Ca	20	0.004
	1+	^{46}Ti	22	8
	2+	^{92}Zr	40	17.15
	2+	^{92}Mo	42	14.84

However, measurements on cesium sulfate targets (also mixed with iron, niobium and copper) showed that these interferences do not distort ^{135}Ba count rates for 2+ and 3+ charge states as a separation of the events in the detector is feasible (e.g. see Fig. 3.4). Still, tuning is error-prone in cases of intense interferences. In summary, interferences mostly occurred in iron mixed targets, whereas copper mixed targets showed rather clean spectra.

Though, puzzling results were gained for masses 135, 137 and 138 in charge state 2+, since unidentified interferences with lower energy loss than the corresponding Ba^{2+} have been observed on carbon, aluminum and copper targets. In theory, $^{135}\text{Ba}^{2+}$ and $^{137}\text{Ba}^{2+}$ do not possess any m/q interferences. The unknown peak vanished with narrow slits (± 1 mm) in front of the high-energy electrostatic analyzer, but count rates then dropped to 1–2 cnts/s. This suggest that there has been a problem with the tuning. Therefore, following measurements were conducted in the 3+ charge state.

3.2.2. Standard and blank correction

Due to the fact that AMS measurements of cesium have not been performed until now, no standard material for $^{135}\text{Cs}/^{133}\text{Cs}$ or $^{137}\text{Cs}/^{133}\text{Cs}$ at AMS levels is available. In order to determine valid ratios of the HE ^{133}Cs current (measured in an offset

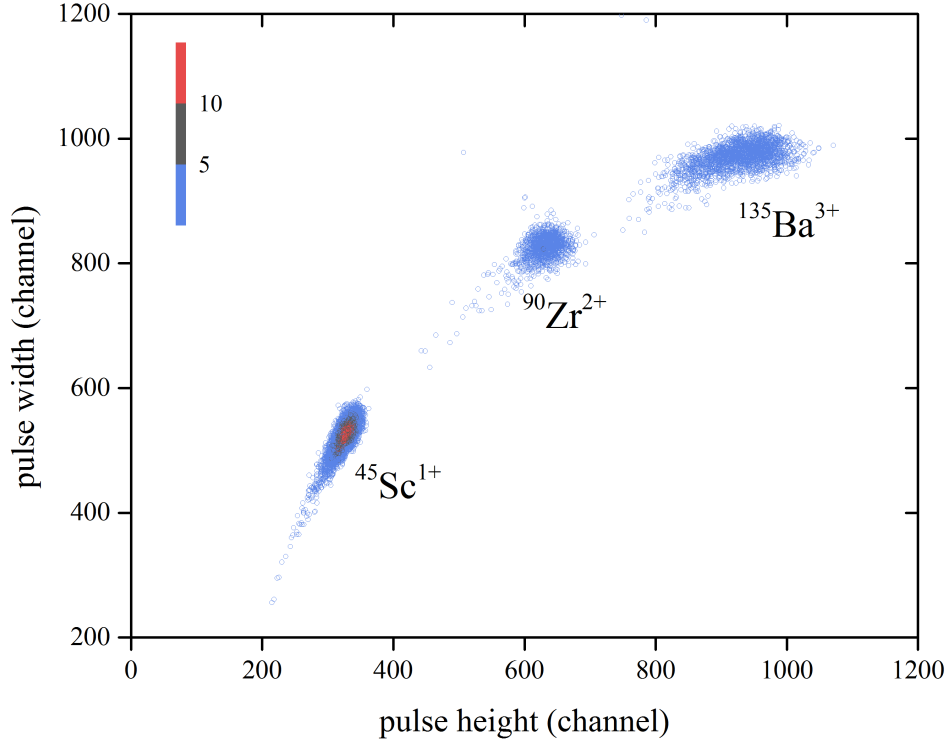


Figure 3.4.: Pulse width vs. pulse height spectrum of cesium sulfate mixed with iron ($\text{Cs}:\text{Fe} = 1:1$ atomic ratio) measured for 185 s in the Bragg detector. Mass over charge interferences for the injected $^{135}\text{Ba}^{3+}$ can be clearly separated. (Measured in Cs1410.)

Faraday cup after the analyzing magnet) and the ^{135}Ba count rate (measured in the Bragg detector and thus additionally passing the electrostatic analyzer, the switching magnet, a second analyzing magnet and quadrupol lenses), a HE transmission correction is required. The assessed transmission from the high-energy side offset cup to the Bragg detector is $(82.1 \pm 4.3)\%$. This value is based on a few single measurements taken in beam time Cs1410 (see Table 3.3), which were combined to the total transmission by calculating the product of the transmission through the high-energy side electrostatic analyzer and the transmission through the remaining components leading to the Bragg detector: $^{133}\text{Cs}^{2+,3+}$ currents presented in Table 3.3 were first measured in the high-energy side Faraday cup fc 04 situated directly after the first analyzing magnet (on the beamline). Then, immediately after opening the cup, the current was measured in Faraday cup fc L4 directly behind the ^{14}C detector (see Fig. 1.1). The currents monitored were stable, therefore this way of determining the transmission is justified. Similarly, count rates were measured in the ^{14}C detector (a silicon semiconductor detector) and in the Bragg detector. Measured atomic ratios in the following have all been scaled by the HE transmission.

3.2. Setup with Bragg detector

Table 3.3.: Data taken for the transmission estimation at 1.6 MV terminal voltage (no shorting rods) in the 2+ charge state and with shorting rods in the 3+ charge state, respectively. The Faraday cup fc 04 is situated directly after the analyzing magnet and fc L4 is located after the high-energy side ESA at nearly the same position as the detector used for ^{14}C measurements. Sample materials were cesium sulfate in a copper cathode for the current measurement and cesium sulfate mixed with copper (1:1 atomic ratio) in a copper cathode for the count rates. (Measurements taken in Cs1410.)

fc 04 [nA]	fc L4 [nA]	transmission
5.10	4.90	0.961
6.10	6.04	0.990
4.93	4.61	0.935
3.44	3.33	0.968
4.98	4.56	0.916
10.50	10.00	0.952
average transmission (95.4 ± 1.1)%		
^{14}C detector [Cnts/s]	Bragg detector [Cnts/s]	transmission
275	255	0.927
240	210	0.875
240	187	0.779
average transmission (86.0 ± 4.4)%		

Further, it has been observed that samples in aluminum cathodes seem to give lower $^{135}\text{Ba}/^{133}\text{Cs}$ ratios than their copper equivalents. One explanation would be that the use of aluminum diminishes barium currents (better than copper). But since Fig. 5.5 shows that barium count rates of comparable aluminum and copper blanks match within their error bars, but cesium currents are by trend higher on aluminum targets, it turns out to be more likely that aluminum cathodes enhance the $^{133}\text{Cs}^-$ current just as it is described in Middleton (1989). This would be a problem, if external cesium — i.e. cesium residues in the source, cross contaminations and impurities in the rubidium used for sputtering — constitute the enhanced $^{133}\text{Cs}^-$ current.

Therefore high-energy ^{133}Cs currents of samples in Al cathodes were corrected with the average ^{133}Cs current on aluminum blanks $\text{HE}(^{133}\text{Cs})_{\text{Al}} = 0.02 \text{ nA}$ (see Table 5.2) in the following way: $\text{HE}(^{133}\text{Cs}) - \text{HE}(^{133}\text{Cs})_{\text{Al}}$.

4. Stripping process

The centerpiece of VERA is the 3 MV tandem accelerator. As the name “tandem” implies, ions are accelerated in two stages. In the middle of the accelerator the terminal is situated, which can be set to a positive potential of 3 MV by two charging chains providing a total charging current of $230\ \mu\text{A}$. First the negative ions are accelerated towards the terminal. There, they have to penetrate either a thin foil or a gas volume. Due to collisions with gas or foil atoms, the singly charged negative ions lose several electrons — a process called stripping. The now positively charged ions experience a second acceleration away from the terminal.

Different cross sections for each charge exchange determine the equilibrium charge state distribution after the accelerator. Although there exists no complete formalism of these processes, some theoretical and semiempirical formulas for the determination of the resulting average charge states in stripping processes have been accomplished by e.g. Betz (1972), Sayer (1977) or Dinev (2009). The charge state distribution depends on the type and pressure of the utilized stripper gas, the cross sections for charge exchange between ions and stripper gas as well as on the velocity of the ions (Niklaus et al., 1994). Choosing a highly populated charge state is a prerequisite to obtain high transmission through the accelerator. Though, the charge state distribution and the transmission for each charge state are not equivalent. The transmission also takes ion optics and general beam transport for each charge state into account, but of course correlates with the charge state distribution. As described in section 3.2, highest possible transmission through the accelerator was the aim in the cesium measurements, which rules out high charge states (e.g. an average transmission through the accelerator of 1.7 % in the 8+ charge state).

4.1. Transmission in He and Ar

4.1.1. Experimental setup

In order to determine the transmission through the accelerator, the currents measured in the Faraday cups in front of the accelerator (LE(^{133}Cs)) and after the analyzing magnet (HE(^{133}Cs)) were recorded, respectively. The resulting transmission is calculated as the ratio of the normed HE and LE currents as displayed in equation 4.1. The parameter q denotes the charge state of the beam particles on the high energy side.

$$\text{TRA} = \frac{\text{HE}(^{133}\text{Cs})}{q \cdot \text{LE}(^{133}\text{Cs})} \quad (4.1)$$

Measurements were taken for different charge states at terminal voltages of 2.0 MV, 2.5 MV and 2.9 MV with helium and argon as stripper gases, respectively. Based on a setup for 2.9 MV and the 3+ charge state, machine parameters were automatically scaled by the script “load setup“ for the wanted terminal voltage and charge state. Fine tuning was done with the help of the automatic optimization script “automax“(Steier, 2000). The script was set to optimize the settings of the Wien filter, the einzel lens and the steerers right in front of the accelerator as well as the steerers after the accelerator in order to maximize the current measured in the HE Faraday cup after the analyzing magnet. It has to be taken into account that the preferred charge state might not yield the maximum HE current. It is advisable to periodically check, whether you are “sitting“on the right peak.

Optimizing the stripper gas pressure was done by carefully regulating the valve of the stripper gas supply. Since the time constant for reaching equilibrium is rather high, LE and HE currents (for calculating the transmission) and the stripper gas pressure were permanently logged for a longer period of time (see Fig. 4.1). The utilized measuring cell is situated on the high-energy end of the accelerator and does not measure the pressure within the stripper, but where the gas effuses. Pressure values are correct for argon and must be scaled by a factor for the respective gas listed in a handbook for the measuring cell¹. This correction was not made for helium, as the actual pressure value was not of relevance.

A possibility to improve ion optics in the accelerator at lower terminal voltages (2.0 MV or less) is the implementation of shorting rods. With the application of shortening an enhancement of transmission by a factor of 1.2 is feasible. Though, the presented data was taken without the use of shorting rods.

4.1.2. Results

The currents were recorded after burn-in time (i.e. the time the target surface needs to condition for providing a stable current when being sputtered; waiting time was approx. 1 min for each measurement) on four different cesium sulfate targets in aluminum cathodes. The transmission values shown in Table 4.1 are mean values. A data visualization is given in Fig. 4.2 and Fig. 4.3. When employing Ar as stripper gas, best transmission is clearly gained by choosing the 2+ charge state, reaching values of 23% to 28% (depending on the ion energy). However, with He, also higher charge states show good or even better transmission (e.g. up to 24% for the 3+ at 2.9 MV terminal voltage). As expected (from the Sayer-formula, see section 4.2.2) lower

¹No scaling is needed for Air and N₂. The scale factors for other gases are 5.56 for He, 9.90×10^{-1} for O₂ and 7.75×10^{-1} for Ar.

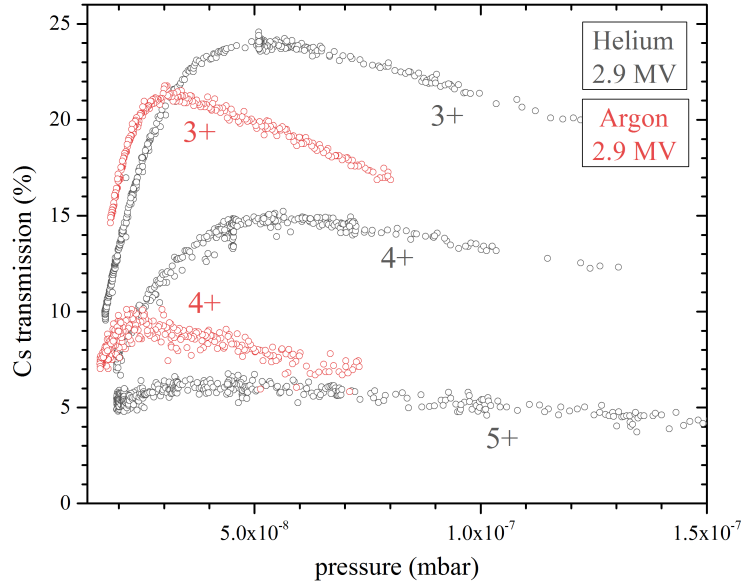


Figure 4.1.: Recording of the transmission through the accelerator at varying stripper gas pressure (helium and argon, 2.9 MV terminal voltage) for charge states 3+, 4+ and 5+. The HE current for the calculation of the transmission was measured in a Faraday cup after the analyzing magnet. (Measurement taken in Cs1408.)

terminal voltages (i.e. lower ion energies) are favorable to achieve higher yields in the 2+ charge state, whereas higher terminal voltages are beneficial for higher charge states. Also, in Fig. 4.2 and Fig. 4.3 a comparison of the transmission measurements with measured equilibrium fractions for iodine (G Ryding and A B Wittkower and P H Rose, 1969) is shown. Equilibrium fractions are generally higher than the transmission values, which is due to the included losses because of e.g. ion optics. The equilibrium fractions predict a higher transmission of the 4+ charge state with He than measured. With O₂ as stripper gas, 26.9% for the 3+ charge state for iodine are reported, whereas the measured transmission for cesium in our experiment was approximately 17%. (A comparison of iodine and cesium is reasonable, as their mass and atomic number are similar.)

The relation of transmission and stripper gas pressure has been examined for several charge states (Fig. 4.1). The tendency that helium requires higher densities than argon can be explained by its lower mass and electron density. The cross section for interactions in the stripper medium increases with electron density. Therefore, more helium atoms than argon atoms are needed in the stripper volume to provide the same e⁻ density. As both gases have the same temperature in the stripper, helium atoms move faster than argon atoms and effuse out of the stripper volume more easily. Optimal values for the pressure are ca. 3×10^{-8} mbar for Ar and

approximately 5×10^{-8} mbar² for He.

Table 4.1.: Average transmission through the accelerator of a selection of manual measurements at different settings for terminal voltage, charge state and stripper gas. Gas pressure in the stripper was at its optimal value of approx. 3×10^{-8} mbar for Ar and slightly higher at 5×10^{-8} mbar for He, respectively. Some transmission values are based upon a single measurement and therefore no experimental standard deviation can be calculated. (Measurements taken in Cs1408.)

Terminal voltage	q	TRA in He	TRA in Ar
2.0 MV	2+	(27.4±0.1)%	(28.6±0.4)%
	3+	(17.3±1.1)%	(13.3±0.7)%
	4+	(9.8±0.1)%	(4.6±0.3)%
2.5 MV	2+	(21.2±0.3)%	25.0%
	3+	(23.7±0.5)%	(19.2±0.6)%
	4+	(14.0±0.3)%	(9.4±0.1)%
2.9 MV	2+	(20.7±0.4)%	(23.5±0.6)%
	3+	(24.4±0.3)%	(20.5±0.3)%
	4+	(13.35±0.6)%	8.8%
	5+	(5.4±0.1)%	3.4%

4.2. Charge state distribution in He and Ar

A convenient method to measure the charge state distribution of a particle beam at a specific setup (terminal voltage, stripper gas, pressure) at VERA is by means of the Wien filter. Though, it has to be considered that contributions of ion optics and transmission of both, accelerator and Wien filter, affect the measurement. Hence, the measured charge distribution might deviate slightly from the true distribution.

The basic idea of a Wien filter is to compensate the Lorentz force of a particle with electric charge q traversing a homogeneous magnetic field B and an orthogonal electric field E . As equation 4.2 illustrates, this can be achieved for one particular velocity v :

$$qE = qvB \quad (4.2)$$

²As outlined in section 4.1.1, this value only gives the reading of the pressure measurement.

4.2. Charge state distribution in He and Ar

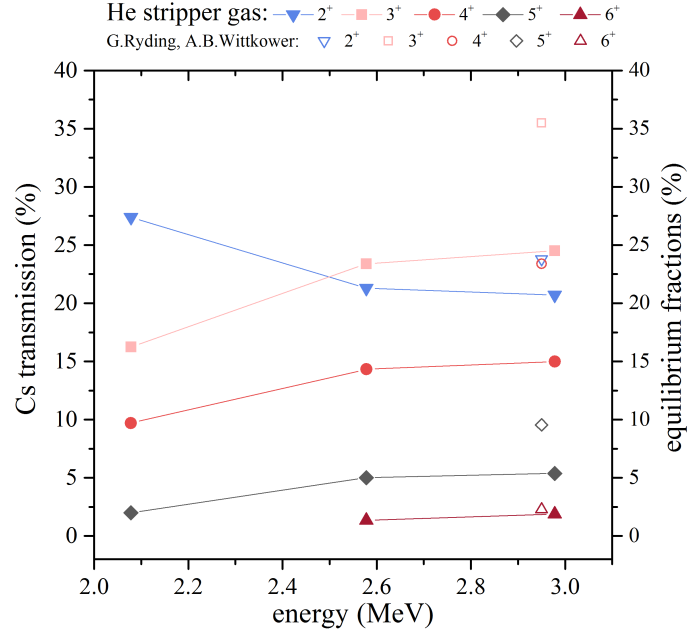


Figure 4.2.: Transmission through the accelerator at different ion energies at the terminal for He stripping. In order to adjust for losses due to different ion optics of the charge states, lenses and steerers were tuned in each case. No shorting rods were applied. Measurements are compared to the equilibrium fractions for iodine measured by G Ryding and A B Wittkower and P H Rose (1969). (Measured in Cs1408.)

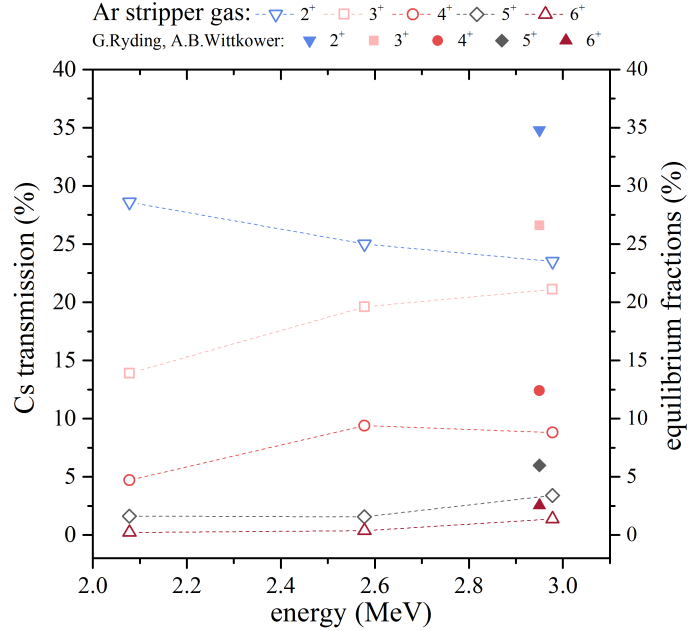


Figure 4.3.: Transmission through the accelerator at different ion energies at the terminal for Ar stripping. Measurements are compared to the equilibrium fractions for iodine measured by G Ryding and A B Wittkower and P H Rose (1969). (Measured in Cs1408.)

Hence, ions at velocity $v = E/B$ traverse the Wien filter undeflected. The particle energy \mathcal{E} after the accelerator is determined by equation 4.3 for the charge state q , whereas M and m are the masses of the injected molecule and the ion of interest analyzed on the high-energy side, respectively. Since all parameters of equation 4.3, except for q , are given and distinct, the Wien filter not only acts as a velocity selector, but may also be used as a charge state selector.

$$\mathcal{E} = \frac{m}{M} (U_{\text{source}} + U_{\text{terminal}}) + U_{\text{terminal}} \cdot q = \frac{mv^2}{2} \quad (4.3)$$

Varying the electric field of the Wien filter at constant magnetic field therefore offers a convenient way to separate different charge states. For that purpose, the particle current is measured in the Faraday cup between accelerator and analyzing magnet. Different charge states then correspond to clearly separated peaks in the recorded Wien filter scan (see Fig. 4.4).

4.2.1. Experimental setup

Wien filter scans have been made at three different terminal voltages (2.0 MV, 2.5 MV and 2.9 MV) with helium and argon stripping, respectively. The slits in front of the Faraday cup have to be narrowed (1 – 1.5 mm) to reach a sufficient resolution of the peaks. Focussing is only possible for one charge state at a time. Hence, lenses, steerers and the Wien filter voltage were first tuned manually and then optimized with the automatic tuning script “automax“ for each charge state. This improves the transmission on the selected charge state and decreases transmission for the others. (In Fig. 4.4 the influence of focussing for one particular charge state, with the remaining settings held constant, can be seen.) It has to be considered that for full comparability of the currents measured for each charge state, a charge standardization is required (i.e. the current measured in the Faraday cup divided by the respective charge state). Thus, the only information gained of Fig. 4.4 is that focussing improves ion optics for the respective charge state tuned for, but no conclusions regarding yield or charge state distribution can be drawn without further evaluation.

4.2.2. Comparison with Sayer’s model

In the review by Sayer (1977) semiempirical formulas for heavy-ion stripping based on extensive charge state measurements are presented. An asymmetric function

$$F_q = F_m \cdot \exp \left(\frac{-0.5 \cdot t^2}{1 + \varepsilon t} \right), \quad (4.4)$$

4.2. Charge state distribution in He and Ar

where $t = (q - q_0)/p$ and q_0 is the charge value with maximum intensity was fit to each experimental charge state distribution. Data was evaluated for the most common stripping media, i.e. carbon foils and dilute light gases. B.L. Doyle from the Sandia National Laboratories has built a calculation program for charge state distributions based on equation 4.4. Approximate values to describe an average dilute gas for the parameters in equation 4.4 were used.

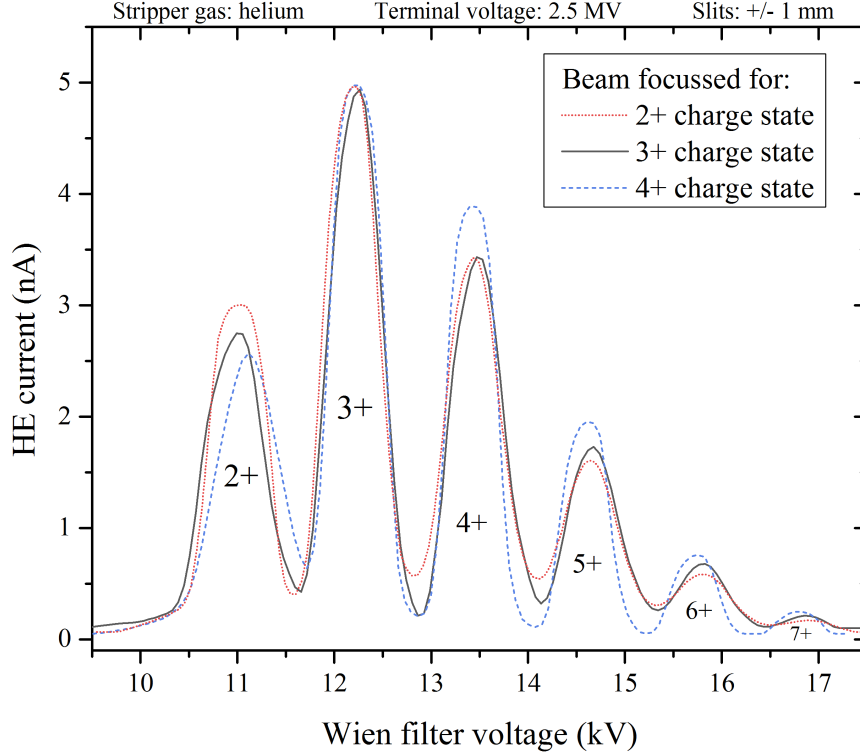
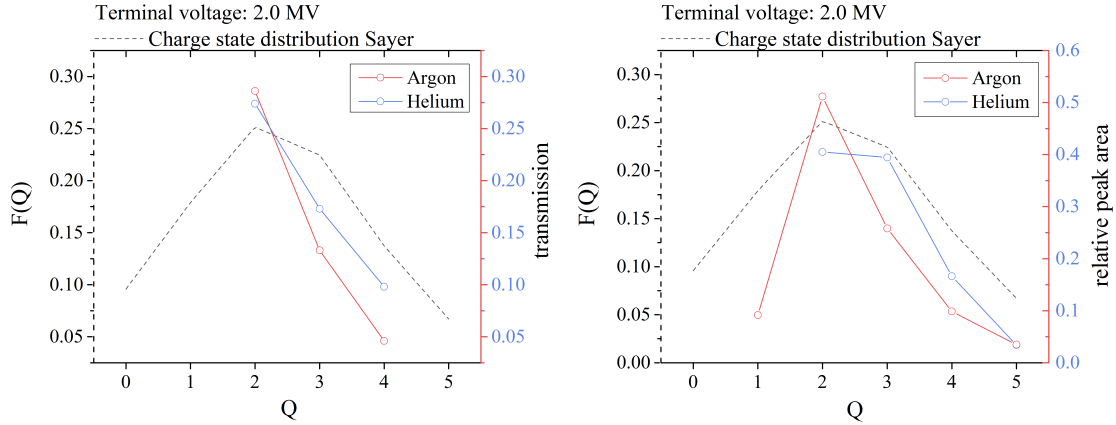


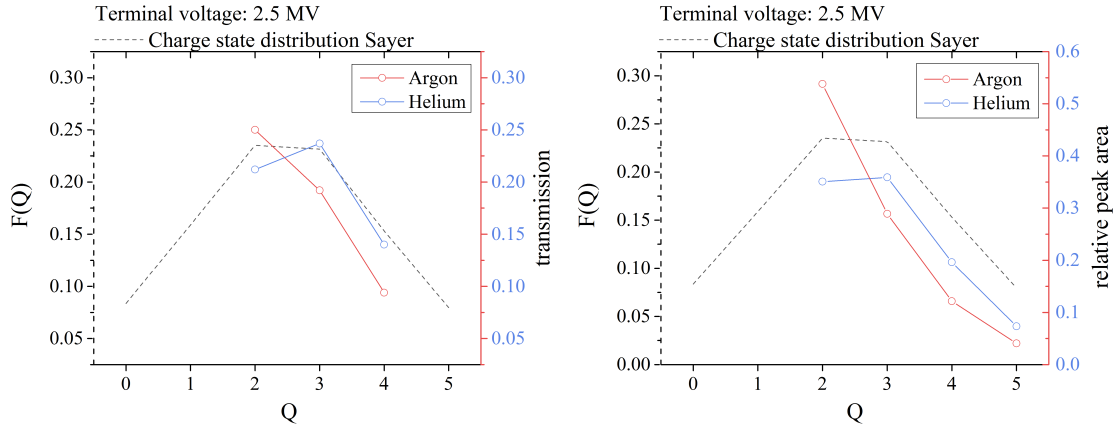
Figure 4.4.: Wien filter scan with optimized settings for different charge states. Scans for the charge states 2+ and 4+ were shifted and scaled with respect to the 3+ peak of the 3+ scan to facilitate comparison of the relative heights of the peaks (2+: $(0.05 \text{ kV} + x : 0.65 \times y)$; 4+: $(-0.70 \text{ kV} + x : 0.52 \times y)$). The HE current was measured in the Faraday cup directly after the accelerator. The peak heights are not adjusted for the respective charge state. (Measured in Cs1408.)

The charge state distribution for injecting Cs^- at a terminal voltage of 2.0 MV, 2.5 MV and 2.9 MV was computed with this program, respectively. In Fig. 4.5a, 4.6a and 4.7a comparisons of the predicted and the measured charge state distributions are shown (values from Table 4.1). The measured fraction of each charge state is affected by ion optics and variations of stripper gas properties. Therefore no complete conformity of model and measurement can be expected. Nevertheless, both, calculated and measured distributions, favor the 2+ and 3+ charge states.



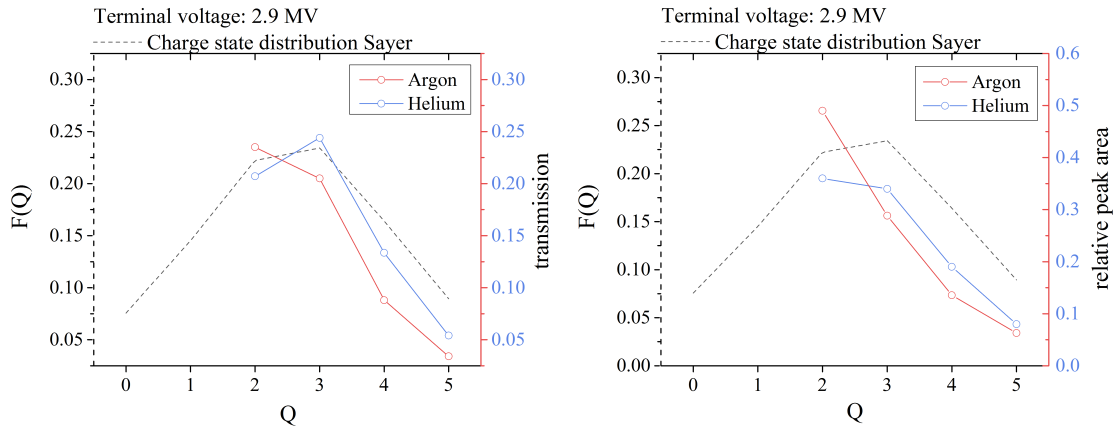
(a) Transmission for each charge state compared to the charge state distribution. (b) Relative peak areas of WF scans compared to the charge state distribution.

Figure 4.5.: Charge state distribution at 2.0 MV terminal voltage.



(a) Transmission for each charge state compared to the charge state distribution. (b) Relative peak areas of WF scans compared to the charge state distribution.

Figure 4.6.: Charge state distribution at 2.5 MV terminal voltage (Cs1408).



(a) Transmission for each charge state compared to the charge state distribution. (b) Relative peak areas of WF scans compared to the charge state distribution.

Figure 4.7.: Charge state distribution at 2.9 MV terminal voltage (Cs1408).

In Fig. 4.5b, 4.6b and 4.7b the calculated distributions are compared to the distributions resulting from the relative, charge normed areas of the peaks in the respective Wien filter scans (focussed for the 2+ charge state). Losses due to neutralization of ions (and also bad ion optics) are not taken into account. Therefore charge state fractions of the Wien filter scans are higher compared to their calculated correspondent (and to normally measured transmissions with AMS). Though, the distributions resemble each other in shape. Sayer's formula (equation 4.4) seems to render the measured data for helium in a more appropriate way than for argon.

5. Ratio measurements

The result of an AMS measurement is an isotopic ratio, i.e. the ratio of the number of the rare isotope and the number of its (abundant) sister isotope in a sample. The particular aim of cesium AMS measurements is to determine the ratios $^{135,137}\text{Cs}/^{133}\text{Cs}$ and $^{135}\text{Cs}/^{137}\text{Cs}$ in unknown samples. Though, as long as no full suppression of the barium isobars is provided, count rates on mass 135 amu and 137 amu have to be assigned to $^{135,137}\text{Ba}$. However, measuring the atomic ratios $^{135,137}\text{Ba}/^{133}\text{Cs}$ of both, cesium and blank samples, at least gives an estimate of the purity of the used materials, partial isobar suppression in various steps of the measuring procedure and the detection limit of the setup, respectively.

5.1. Measured atomic ratios

$^{135}\text{Ba}/^{133}\text{Cs}$ ratios have been measured for several materials to test the purity of cesium compounds, matrices and cathodes. Copper proves to be preferable for both cathode and mixing material. Due to its superior performance in the ion source (section 2.2), cesium sulfate is the compound of choice instead of cesium chloride. For that reason cesium chloride samples were not measured in the detector.

Copper as a matrix for cesium sulfate has been examined in three atomic mixing ratios: $\text{Cs}:\text{Cu} = 1:1$, $1:3$ and $1:10$. These measurements were conducted in the $2+$ charge state at 1.6 MV terminal voltage with helium as stripper gas, all slits open and an average transmission of 18% through the accelerator (Cs1409). Barium impurities rather stem from copper powder than from the used cesium sulfate (purity 99.997%) (both Alfa Aesar), as the barium ratio increases (unproportionally) with copper content (see Table 5.1 and Fig. 5.1). Anyway, pure cesium sulfate performs better concerning intensity of current, but mixing with copper powder remains a good alternative for small sample sizes.

To examine the influence of the target preparation (including cleaning tools, mixing samples and pressing targets) under usual laboratory conditions, cesium sulfate was first diluted in purified water (milli-Q) and then dried on a heating plate. Afterwards it was mixed with copper (1:3, atomic ratio) and pressed into a copper cathode in the same way as the other samples. Within their uncertainties, for copper there is no discrepancy between diluted and non-diluted Cs_2SO_4 samples (Fig. 5.1).

Iron and niobium in different mixing ratios were tested for output (section 2.2.1) and for their barium content (see Table 5.1 and Fig. 5.2). However $^{135}\text{Ba}/^{133}\text{Cs}$ ratios are higher by orders of magnitude, which indicates inherent impurities of these materials. Therefore they are no adequate alternative to copper.

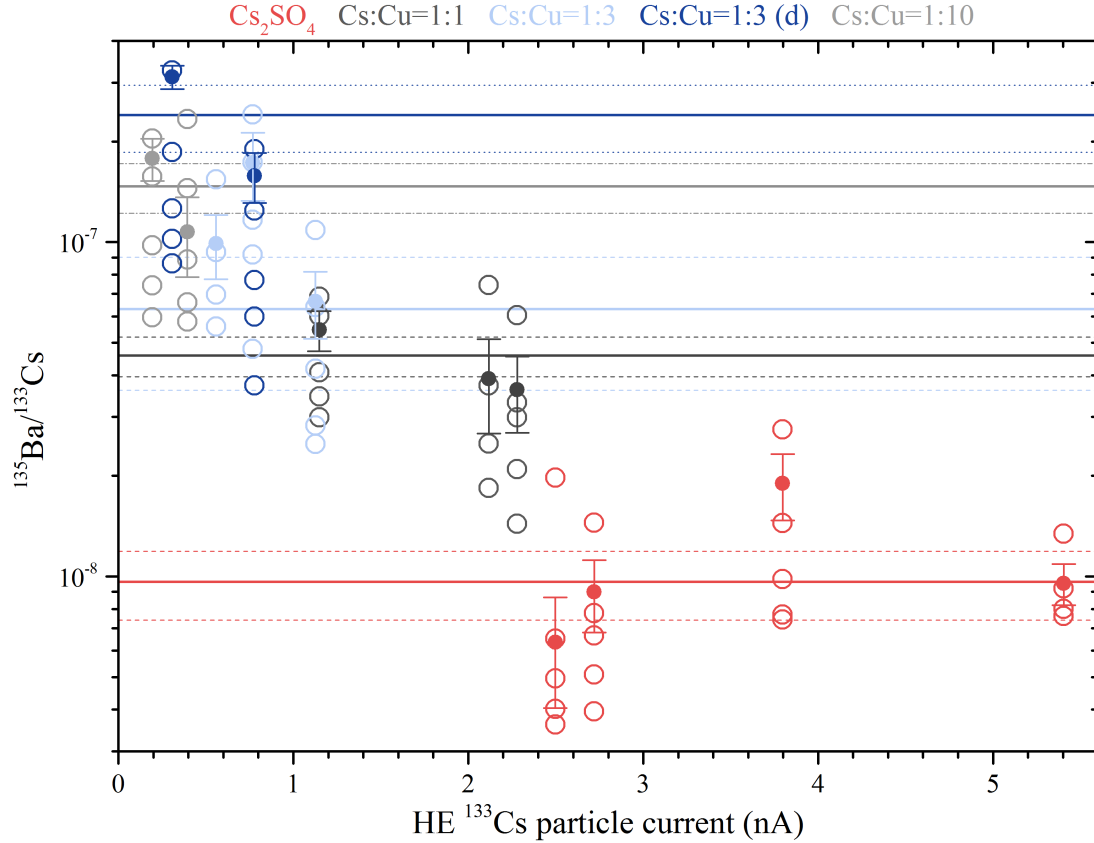


Figure 5.1.: Measured $^{135}\text{Ba}/^{133}\text{Cs}$ ratios for several copper mixed targets relative to the HE current (Cs1409). The empty circles refer to ratios per run (uncertainties are smaller than the size of the circles), the filled circles represent the average values for each cathode and the solid horizontal lines are the average ratio for each material (dashed/dotted lines show uncertainties). In each run a sample was measured for approximately 95 s. Some 1:3 mixed samples were diluted and dried before pressing and are marked with (d). The top data point for each measurement is significantly higher than the lower ones — this always is the first run on the particular cathode and its higher $^{135}\text{Ba}/^{133}\text{Cs}$ ratio could be explained by surface contaminations, which are cleaned off in the sputtering process. Another explanation is the change of thermal conditions over sputter time, which would also explain, why the contamination is not identical on mixed and pure samples, as a copper matrix improves thermal conductivity in the sample. Nevertheless, all runs are included in the mean value.

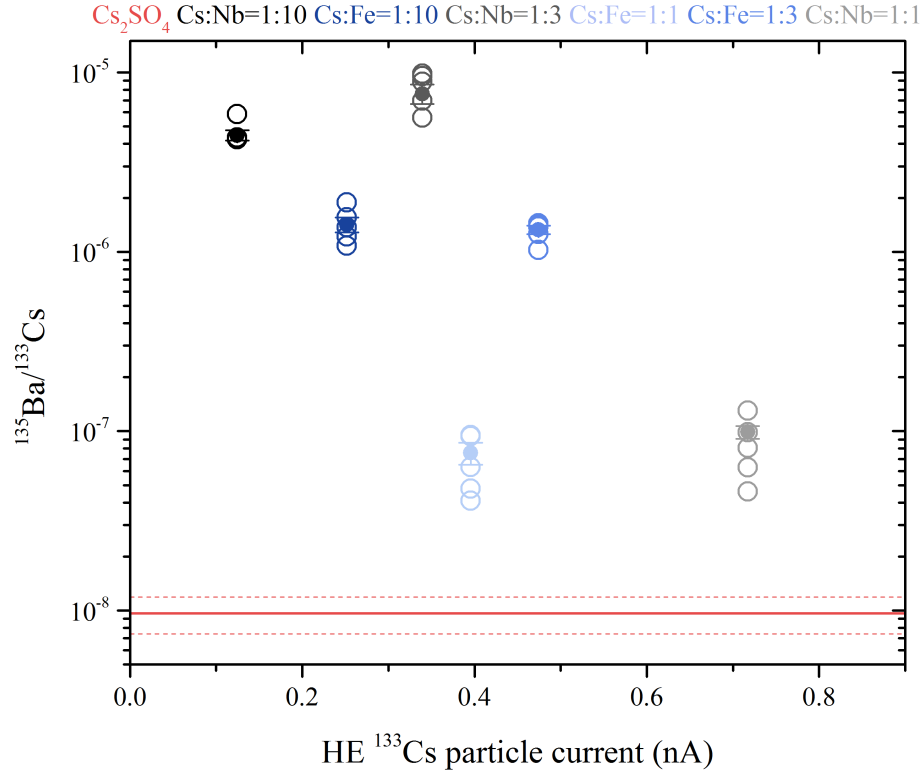


Figure 5.2.: Measured $^{135}\text{Ba}/^{133}\text{Cs}$ ratios for several iron and niobium mixed targets (Cs1409). The empty circles refer to ratios per run (uncertainties are smaller than the size of the circles), the filled circles represent the average values for each cathode and the solid red line is the average ratio for Cs_2SO_4 (copper cathode) (dashed lines show uncertainties). In each run a sample was measured for approximately 95 s.

Table 5.1.: High-energy cesium particle current ^{133}Cs ($2+$), $^{135}\text{Ba}^{2+}$ counts per second and the atomic ratio $^{135}\text{Ba}/^{133}\text{Cs}$. Measurements were taken in Cs1409. The internal error of the average $^{135}\text{Ba}/^{133}\text{Cs}$ is calculated with the uncertainties of the ratios for each target.

material	cat.	#	^{133}Cs [pA]	$^{135}\text{Ba}^{2+}$ [1/s]	$^{135}\text{Ba}/^{133}\text{Cs}$	int. error	ext. error
Cs_2SO_4	Cu	4	3600 ± 360	225 ± 41	0.97×10^{-8}	0.10×10^{-8}	0.23×10^{-8}
CsCu11	Cu	3	1830 ± 240	415 ± 64	4.58×10^{-8}	0.53×10^{-8}	0.63×10^{-8}
CsCu13	Cu	3	836 ± 76	466 ± 100	6.3×10^{-8}	1.2×10^{-8}	2.7×10^{-8}
CsCu13d	Cu	2	540 ± 120	480 ± 170	24.0×10^{-8}	1.9×10^{-8}	5.5×10^{-8}
CsCu110	Cu	2	290 ± 40	219 ± 51	14.7×10^{-8}	2.0×10^{-8}	2.5×10^{-8}
CsFe11	Al	1	396 ± 31	173 ± 39	7.6×10^{-8}	1.1×10^{-8}	-
CsFe13	Al	1	474 ± 48	3900 ± 500	132.7×10^{-8}	7.1×10^{-8}	-
CsFe110	Al	1	252 ± 42	2190 ± 310	142×10^{-8}	14×10^{-8}	-
CsNb11	Al	1	720 ± 200	400 ± 140	604.3×10^{-8}	0.9×10^{-8}	-
CsNb13	Al	1	340 ± 80	16100 ± 2200	761×10^{-8}	94×10^{-8}	-
CsNb110	Al	1	124 ± 37	3600 ± 1200	447×10^{-8}	30×10^{-8}	-

In order to compare atomic ratios measured on aluminum and copper mixed targets as well as on pure cesium sulfate in aluminum and copper cathodes, respective samples were analyzed in beam time Cs1504c (see Table 5.2 and Fig. 5.5). These measurements were taken at 2.7 MV terminal voltage with O₂ as stripper gas at an average transmission of 10% to 15%. As already explained in section 3.2.2, aluminum cathodes yield a decreased $^{135}\text{Ba}/^{133}\text{Cs}$ ratio of 1.6×10^{-9} for cesium sulfate as compared to 9.4×10^{-9} for the use of the same material in copper cathodes. But considering that the copper blank ((5.5 ± 0.6) pA ^{133}Cs (particle current), (4.9 ± 0.7) $^{135}\text{Ba}^{2+}/\text{s}$) yields both, less cesium and less barium than the aluminum blank ((35.5 ± 3.8) pA ^{133}Cs , (7.8 ± 1.5) $^{135}\text{Ba}^{2+}/\text{s}$), it is the better choice concerning impurities. Fig. 5.3 shows the time development of the HE ^{133}Cs particle currents on the aluminum and copper blanks, respectively. Disregarding any tunings, currents on all cathodes were stable. The adjustment of some machine parameters after sputtering for 100 minutes especially enhances the current of the aluminum blank on position 31. Reasons could be bad focussing particularly for this position or cesium residues in the source, which are released by turning up the line heater and mobilized by sputtering the aluminum target as described in Middleton (1989).

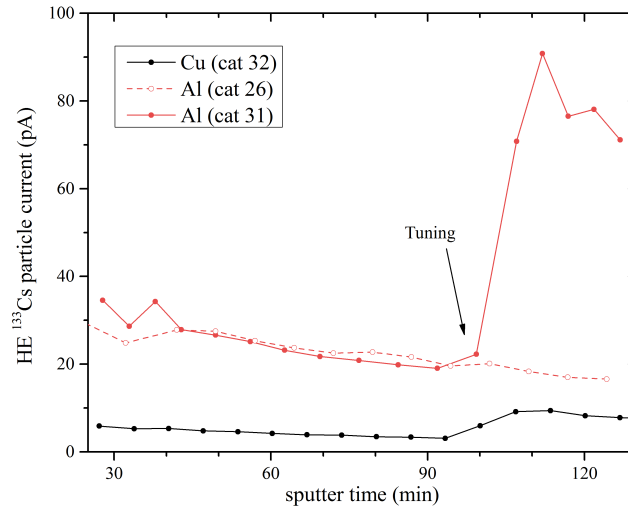


Figure 5.3.: Time development of the HE ^{133}Cs particle current on a copper and two aluminum blanks, respectively. After sputtering for approximately 100 minutes, the focus lens of the ion source was tuned and the current supplying the line heater was turned up from 20 A to 24 A. Tuning and increase of the ionizer power have most effect on the current coming from the aluminum blank on position 31 of the sample wheel. Aside from this, currents are quite stable. Measured in Cs1504c.

Furthermore, it has been observed that $^{135}\text{Ba}/^{133}\text{Cs}$ ratios decrease with sputter time (e.g in Fig. 5.4). Rubidium sputtering cleans the target wheel by removing surface contaminations (barium) in the course of a beam time. This effect is visible in Fig. 5.1 and Fig. 5.2, as the top circles represent the first run per measurement (this is not labelled in the plot). In the shown example in Fig. 5.4 the ^{133}Cs cur-

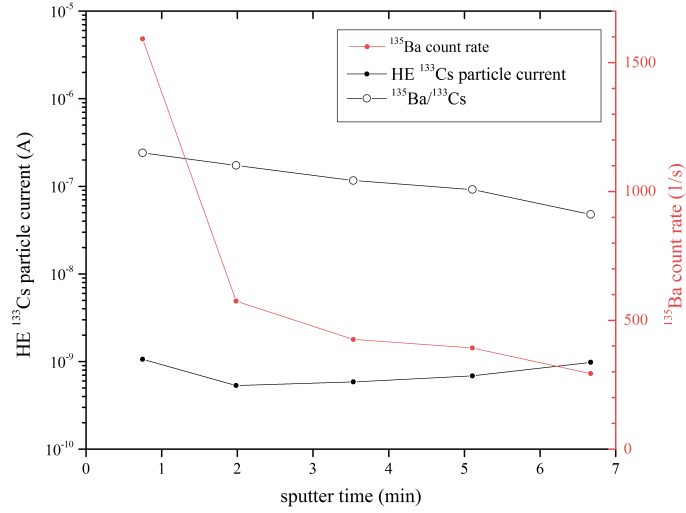


Figure 5.4.: Runs during a measurement in beam time Cs1409 on a cesium sulfate copper mixed sample (Cs:Cu = 1:3, atomic ratio). $^{135}\text{Ba}/^{133}\text{Cs}$ ratios decrease due to decreasing barium count rates and increasing HE current.

rent slightly increases with time, which also decreases the atomic ratio. Generally, $^{135}\text{Ba}/^{133}\text{Cs}$ ratios have been slightly higher in beam times, in which barium samples were mounted in the target wheel (Cs1402-Cs1409).

5.2. Detection limit

Assuming the used chemicals do not contain any ^{135}Cs , they may act as a ^{135}Cs blank for each material, where mass 135 counts are aroused by ^{135}Ba . According to Currie (1968) a blank material's standard deviation σ_B provides an estimate for the detection limit L_D .

$$L_D \approx 3\sigma_B \quad (5.1)$$

The detection limits correlate with the measured $^{135}\text{Ba}/^{133}\text{Cs}$ ratios (Fig. 5.5). Hence best results are gained with cesium sulfate samples in aluminum targets with detection limits down to 2×10^{-9} . In accordance to all previous results, the detection limit is slightly higher for copper mixed samples than for aluminum mixed samples. Overall, detection limits are in the range of 2×10^{-9} to 7×10^{-9} (Fig. 5.5, Table 5.2), which is in the same order of magnitude as the ratios measured in environmental samples by Lee et al. (1993) ($^{135}\text{Cs}/^{133}\text{Cs} \approx 10^{-9}$).

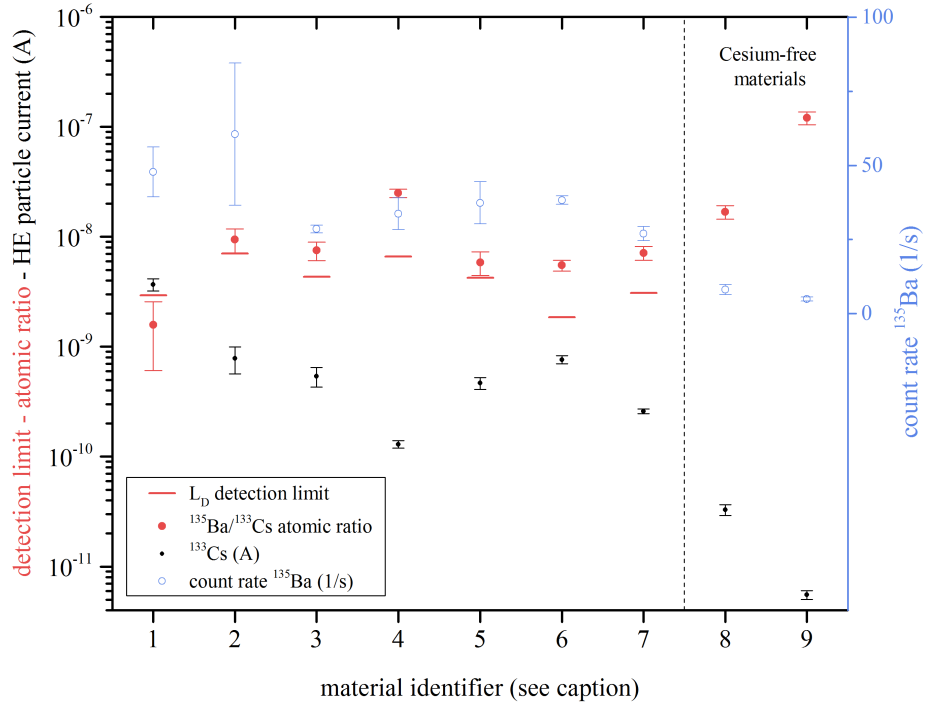


Figure 5.5.: Detection limit, atomic ratio $^{135}\text{Ba}/^{133}\text{Cs}$, ^{135}Ba count rate and Cs^{3+} current for several materials: **1** - Cs_2SO_4 in Al, **2** - Cs_2SO_4 in Cu, **3** - Cs:Cu=1:3, **4** - Cs:Cu=1:10 (each in copper cathodes), **5** - Cs:Al=1:1, **6** - Cs:Al=1:3, **7** - Cs:Al=1:10, **8** - Al (each in aluminum cathodes), **9** - Cu in Cu.

Table 5.2.: Estimation of the detection limit L_D for various samples according to equation 5.1 and the parameters used for calculation: high-energy cesium particle current ^{133}Cs (3+), $^{135}\text{Ba}^{3+}$ counts per second and the atomic ratio $^{135}\text{Ba}/^{133}\text{Cs}$. As the external error was larger than the internal error for all samples, it was used as σ_B in the calculation of L_D . Values for the aluminum mixed samples are corrected to the aluminum-induced cesium current. Measurements were taken in beam time Cs1504c.

material	cat.	#	^{133}Cs [pA]	$^{135}\text{Ba}^{3+}$ [1/s]	$^{135}\text{Ba}/^{133}\text{Cs}$	ext. error	int. error	L_D [10^{-9}]
Cs_2SO_4	Al	5	3690 ± 480	47.8 ± 8.4	1.58×10^{-9}	0.98×10^{-9}	0.66×10^{-10}	2.9
Cs_2SO_4	Cu	2	780 ± 220	61 ± 24	9.4×10^{-9}	2.4×10^{-9}	4.9×10^{-10}	7.1
CsAl11	Al	2	467 ± 58	37.4 ± 7.1	5.9×10^{-9}	1.5×10^{-9}	3.7×10^{-10}	4.2
CsAl13	Al	2	762 ± 66	38.3 ± 1.4	5.50×10^{-9}	0.62×10^{-9}	3.3×10^{-10}	1.9
CsAl110	Al	5	259 ± 14	27.0 ± 2.4	7.1×10^{-9}	1.1×10^{-9}	3.1×10^{-10}	3.1
CsCu13	Cu	1	540 ± 110	28.5 ± 1.3	7.5×10^{-9}	-	15×10^{-10}	4.3
CsCu110	Cu	2	130 ± 10	33.7 ± 5.4	24.9×10^{-9}	2.3×10^{-9}	21×10^{-10}	6.6
Al ¹	Al	2	32.9 ± 3.8	8.1 ± 1.7	16.8×10^{-9}	2.4×10^{-9}	17×10^{-10}	
Cu ¹	Cu	1	5.5 ± 0.6	5.9 ± 0.7	121×10^{-9}	-	170×10^{-10}	

¹ metal powder

5.3. Efficiency

A lower limit for the efficiency of the measurements was determined by sputtering nine targets for approximately 1.5 hours (Fig. 5.6). For this purpose, aluminum cathodes containing pure cesium sulfate, a 1:10 copper mixture and a 1:10 aluminum mixture with a known amount of sample material were prepared (each sample with an initial weight of 1–3 mg cesium sulfate). In order to weigh the sample, the (at first empty) cathode was weighed before and after pressing and the weight of the sample material was calculated as the difference of the two weights. The high-energy current $HE(Cs^{3+})$ measured in the Faraday cup after the analyzing magnet was converted into the respective number of Cs^{3+} ions by equation 5.2, where t_s denotes the sputter time, e the elementary electric charge and N_A the Avogadro constant.

$$N_m(Cs^{3+}) = \frac{HE(Cs^{3+}) \cdot t_s}{3 \cdot e} \quad (5.2)$$

The efficiency then was calculated as the ratio $N_m(Cs^{3+})/N_0(Cs)$ of measured cesium ions and the approximate number of cesium atoms pressed into the cathode. As outlined in equation 5.3, $N_0(Cs)$ can be calculated by comparing the amount of cesium sulfate $m(Cs_2SO_4)$ [mg] with the molar mass $M(Cs_2SO_4)$ [mg/mol] of the compound.

$$N_0(Cs) = \frac{2 \cdot m(Cs_2SO_4)}{M(Cs_2SO_4)} \cdot N_A \quad (5.3)$$

The corresponding data and results are summarized in Table 5.3. The average efficiency of the measurement on nine different cathodes could be estimated to $\geq 5.8 \times 10^{-6}$ (external error 2.7×10^{-6} , internal error 0.007×10^{-6}). The efficiency was best for one particular pure cesium sulfate target with $\approx 27 \times 10^{-6}$. However, the better performance could not be assigned to better sputtering, as sputtering craters on all targets looked similar. Therefore this value is treated as an outlier. A better estimation could have been reached by sputtering the targets for a longer period of time, as there is still sample material left in all cathodes.

5.4. Sequenced measurement

At VERA, it is possible to sequentially inject different isotopes in the detector, as the configurations of the automatic measurement are highly adaptable. Therefore, by changing the multi beam sequencer, the terminal voltage and the high-energy side ESA for each sequence, ions of mass 135, 137 and 138 amu can be detected in one run, respectively. On the one hand, the nearly simultaneous measurement of masses 135 amu and 137 amu allows for determining the ratio $^{135}X/^{137}X$ and on the

CHAPTER 5. Ratio measurements

Table 5.3.: Measurements and calculations for the efficiency of cesium measurements. The numbers of cesium ions (N_m) and atoms (N_0) were computed according to equation 5.2 and 5.3, respectively. The error of N_m is negligible (relative error $< 10^{-8}$), the error of the weighted samples is < 0.02 mg.

sample	Cs ₂ SO ₄	matrix	$N_m[10^{13}]$	$N_0[10^{18}]$	t_s (min)	$N_m/N_0[10^{-6}]$
Cs ₂ SO ₄	3.06 mg	-	27.4	10.18 ± 0.05	50.46	26.95 ± 0.12
Cs ₂ SO ₄	1.67 mg	-	1.96	5.56 ± 0.05	41.62	3.52 ± 0.30
Cs ₂ SO ₄	6.54 mg	-	8.09	21.77 ± 0.05	46.79	3.72 ± 0.01
CsCu110	1.40 mg	4.91 mg	2.74	4.65 ± 0.05	50.24	5.89 ± 0.03
CsCu110	0.78 mg	2.73 mg	0.47	2.59 ± 0.05	45.10	1.79 ± 0.06
CsCu110	0.43 mg	1.52 mg	0.51	1.44 ± 0.05	45.52	3.54 ± 0.12
CsAl110	1.55 mg	2.31 mg	1.18	5.16 ± 0.05	50.32	2.30 ± 0.02
CsAl110	1.35 mg	2.01 mg	0.94	4.49 ± 0.05	47.96	2.08 ± 0.02
CsAl110	1.12 mg	1.67 mg	0.73	3.72 ± 0.05	48.09	1.97 ± 0.03

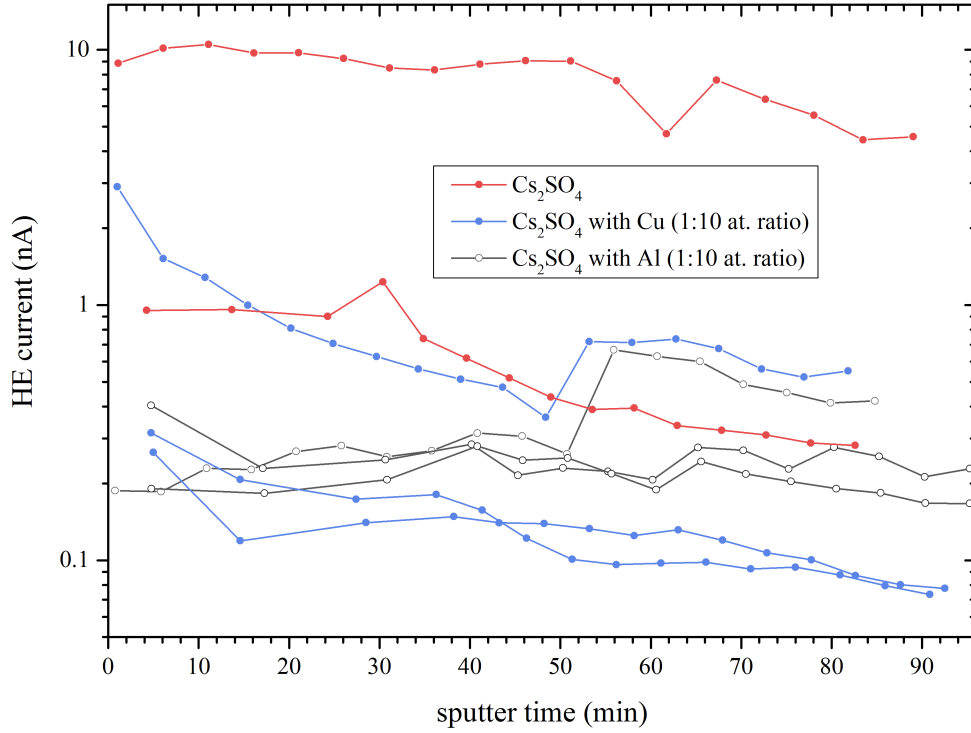


Figure 5.6.: Temporal development of Cs^{3+} particle currents on nine different targets during the efficiency measurement.

other hand, the additional measurement of ^{138}Ba provides a reference value for the barium background. Knowing the isotopic ratios of barium ($^{135}\text{Ba}/^{138}\text{Ba} \approx 0.092$ and $^{137}\text{Ba}/^{138}\text{Ba} \approx 0.157$), discrepancies in the measured values for these ratios can

be recognized and used for a barium background correction.

A setup for a sequenced uranium measurement has been adapted for the use of cesium measurements employing counting times in roughly inverse proportion to the isotopic abundance of each barium isotope (497.5 s for ^{135}Ba , 248.75 s ^{137}Ba and 49.75 s for ^{138}Ba per run, respectively). In Fig. 5.7 a plot of the measured isotopic ratios for several cathodes containing cesium sulfate is pictured. The measured data fits for $^{137}\text{Ba}/^{138}\text{Ba}$ (within 2σ , i.e. 7.2 % relative error), whereas measurements for $^{135}\text{Ba}/^{138}\text{Ba}$ and $^{135}\text{Ba}/^{137}\text{Ba}$ are less accurate and precise (a detailed quantification is given in Table 5.4). The accuracy of a measurement is rated by the difference of its mean value \bar{x} and the true value x_0 , the precision is defined as the standard deviation $\sigma_{\bar{x}}$ of the mean value.

Table 5.4.: Results for barium isotopic ratios of the sequenced measurement. The Symbols denote: true value x_0 for the isotopic ratio, sample mean \bar{x} and standard deviation of the mean value $\sigma_{\bar{x}}$.

isotopic ratio	x_0	\bar{x}	$\sigma_{\bar{x}}$	$\sigma_{\bar{x}}/\bar{x}$	$ x_0 - \bar{x} $	$ x_0 - \bar{x} /x_0$
$^{135}\text{Ba}/^{137}\text{Ba}$	0.59	0.88	0.08	9 %	0.29	49 %
$^{135}\text{Ba}/^{138}\text{Ba}$	0.09	0.12	0.01	8 %	0.03	32 %
$^{137}\text{Ba}/^{138}\text{Ba}$	0.16	0.14	0.01	4 %	0.01	8 %

These results and generally low count rates (≈ 11 counts/s for ^{135}Ba) compared to other beam times (several hundreds) suggest bad tuning (especially for 135 amu) as a reason for the strong scattering and the mismatch with the expected values. Ratios measured on samples not containing cesium fit even less than the presented values. Though, there were no indications for a time trend in the data caused e.g. by terminal voltage fluctuations or sparks in the accelerator. Disregarding the problems due to bad tuning, a barium background correction should be feasible with such a sequenced measurement but requires further experiments.

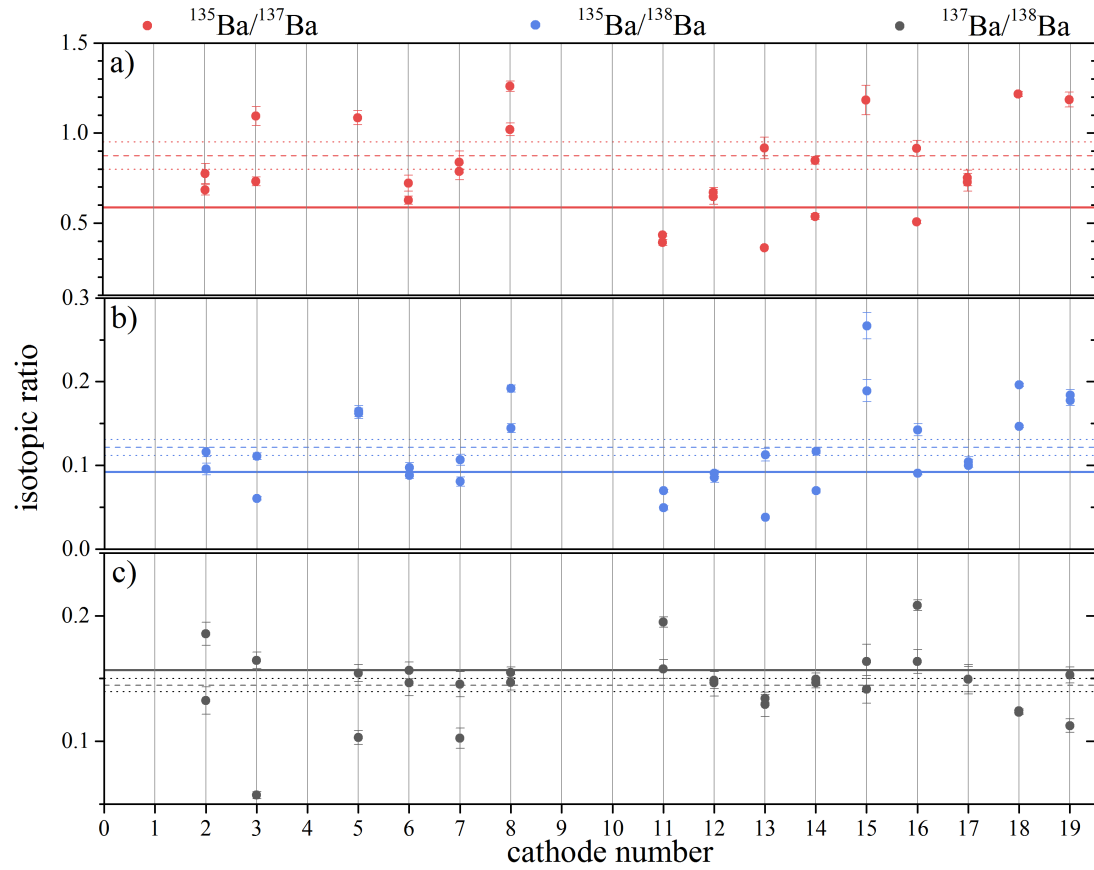


Figure 5.7.: Isotopic ratios a) $^{135}\text{Ba}/^{137}\text{Ba}$, b) $^{135}\text{Ba}/^{138}\text{Ba}$ and c) $^{137}\text{Ba}/^{138}\text{Ba}$ for several samples containing cesium sulfate. The solid lines mark the literature values, the dashed and dotted lines mark average and corresponding uncertainty of all shown points, respectively. (Cs1504b)

6. Conclusions and Outlook

A comprehensive comparison of low-energy currents achieved by sputtering with rubidium ions of ^9Be , ^{12}C , ^{19}F , ^{27}Al and ^{35}Cl was performed. Nearly identical outputs (80%-100%) for both, sputtering with cesium and rubidium ions, showed that rubidium sputtering is a good alternative to cesium sputtering. Rubidium sputtering in combination with cesium sulfate as sample material yielded stable Cs^- currents of up to 60 nA. As barium was found to form stable negative ions (Kaiser et al., 1971), full suppression in the ion source is not possible by injecting Cs^- . Although the average reduction accomplished in the ion source was only $\text{Ba}^-/\text{Cs}^- = 0.4 \pm 0.1$, injecting Cs^- still yielded best results regarding intensity and durability of the LE current compared to other molecules. Mixing a cesium sulfate sample with copper does not significantly deteriorate the Cs^- output — copper therefore is a proper matrix material and preferable compared to iron and niobium. The incorporation of lead(II) fluoride to the sample material led to CsF_2^- currents of several nA, but with a barium suppression of $\text{BaF}_2^-/\text{CsF}_2^- = (8 \pm 3) \times 10^{-2}$ the values presented by Eliades et al. (2013) $\text{BaF}_2^-/\text{CsF}_2^- \approx 5 \times 10^{-4}$ could not be reached. Similar output of CsF_2^- was achieved by using the less hazardous compound LaF_3 . Better mixture of cesium sulfate with the fluoride components. e.g. flushing in HF (MacDonald et al., 2015), has the potential to improve output and barium suppression. The efficiency of the measurements was estimated to be at least 5.8×10^{-6} on pure cesium sulfate samples. The separation of barium and cesium via different energy loss in the MAIC detector is not possible at ion energies reasonably achievable with VERA (26 MeV). Therefore, efforts were made in optimizing beam transport and transmission, which favored lower ion energies (6–12 MeV). After the accelerator, charge states 2+ and 3+ were most populated and resulted in transmissions up to 28%. Tests were carried out with Ar, He and O_2 as stripper gases with no significant differences in transmission. The barium background was least on pure cesium sulfate samples with $^{135}\text{Ba}/^{133}\text{Cs} = (9 \pm 3) \times 10^{-9}$ and $^{135}\text{Ba}/^{133}\text{Cs} = (2 \pm 1) \times 10^{-9}$ in copper cathodes and aluminum cathodes, respectively. This corresponds to detection limits in the range of $2\text{--}7 \times 10^{-9}$ for the isotopic ratio $^{135}\text{Cs}/^{133}\text{Cs}$. Thus, the achieved sensitivity is in the same order of magnitude as the expected ratio in samples proclaimed containing fall-out cesium by Lee et al. (1993). To reach sensitivities needed for natural samples with an expected ratio of $^{135}\text{Cs}/^{133}\text{Cs} \approx 10^{-11}$ (Lachner et al., 2015), further provisions concerning barium suppression are mandatory. The installation of ILIAS will offer new prospects and photodetachment is still to be tested in combination with VERA.

Appendices

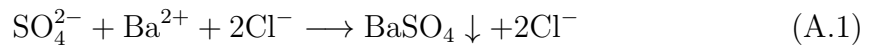
A. Potentials in chemical pretreatment

Up to now, no procedure for a chemical pretreatment of natural samples, supplying (preferably barium free) cesium sulfate for AMS measurements, has been developed. Though, the dissolution of sample material in suitable acids and subsequent precipitation of barium sulfate offers good prospects in both, producing cesium sulfate and removing barium traces.

Also, a practical procedure to estimate the efficiency of the chemical preparation has to be developed. Decay counting of the unstable ^{137}Cs ($T_{1/2} = 30.17$ a) before and after the chemical treatment would allow to evaluate the resulting losses of cesium by comparing the specific activities of the untreated and treated sample material. Since the Chernobyl accident in 1986, the soil in some parts of Austria shows low but still measurable activity arising from ^{137}Cs (Srncik et al., 2008). Therefore suitable material is easily available.

A.1. Precipitation of barium sulfate

Barium sulfate (BaSO_4) is of low solubility (2.448×10^{-4} g/(100 g H_2O) at 20 °C) whereas cesium sulfate (Cs_2SO_4) is highly soluble (179 g/(100 g H_2O) at 20 °C). Therefore BaSO_4 precipitates while Cs_2SO_4 remains in solution. For this purpose cesium chloride (CsCl) and barium chloride dihydrate ($\text{BaCl}_2 \cdot 2\text{H}_2\text{O}$) were dissolved in purified water at a concentration of 0.5 mol/l. Barium chloride and cesium chloride dissociate in water. Therefore the solution contains Ba ions and Cs ions, respectively. As described in equation A.1, the cations SO_4^{2-} react with the available barium (cesium) anions to the salt BaSO_4 (Cs_2SO_4) when sulfuric acid (H_2SO_4) is added to the solution:



In the barium solution, precipitation set in after adding the first drop ($\approx 35 \mu\text{l}$) of 6 molar sulfuric acid with a 1 ml VWR pipette, while in the cesium solution no precipitation took place after adding several drops. After the third drop of sulfuric acid, no further precipitation of barium sulfate was recognized. Hence chemical separation

CHAPTER A. Potentials in chemical pretreatment

of barium sulfate and cesium sulfate should be feasible even at low concentrations. The precipitate can be removed by centrifugation.

As only very little amounts of barium are expected in samples, a matrix for centrifugation would be instrumental for separating the precipitate from the remaining solution. Because of its low solubility (4.43×10^{-3} g/(100 g H₂O) at 20 °C), lead(II) sulfate (PbSO₄) is a suitable material. Thus, a lead(II) nitrate (Pb(NO₃)₂) solution with a concentration of 0.5 mol/l was prepared. Precipitation in the pure solution was tested as well as in mixtures with the barium chloride solution and with both (barium and cesium chloride solutions), respectively. PbSO₄ precipitated after addition of the first drop of sulfuric acid in the pure solution. In the mixed solutions considerably more material precipitated (Fig. A.1).

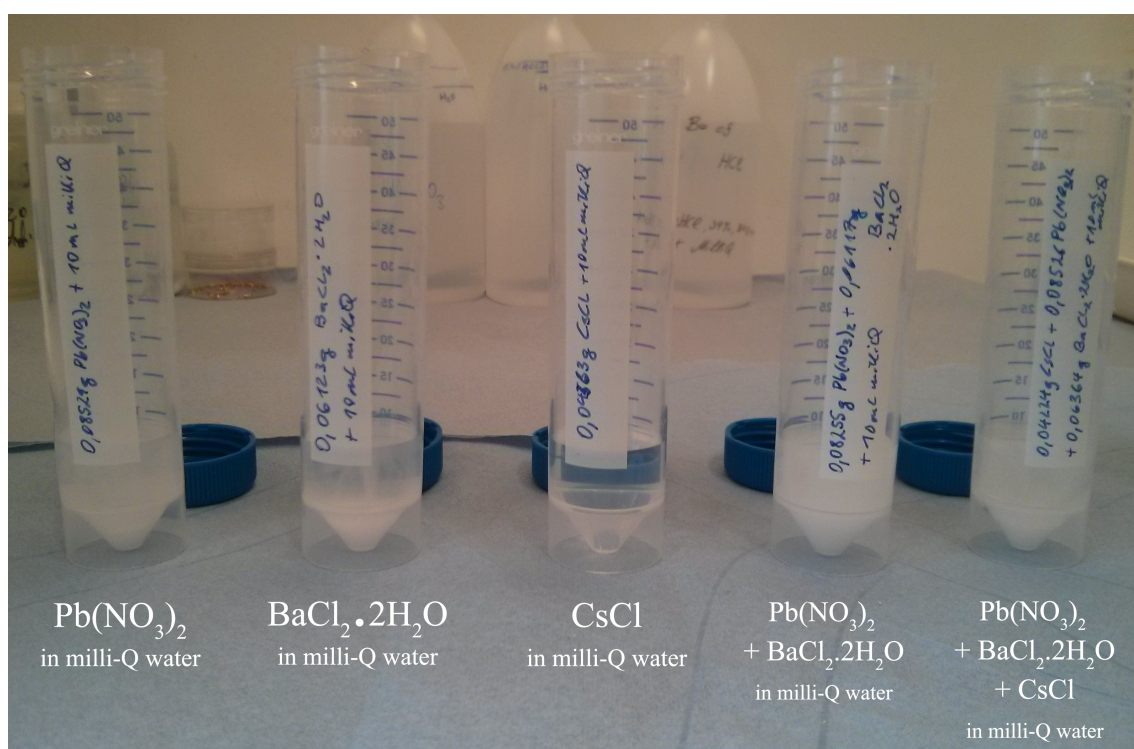


Figure A.1.: Tests on precipitation of barium sulfate. Obviously, the precipitates of the lead(II) nitrate/barium chloride mixtures (the two centrifuge tubes on the right hand side) show the largest quantities of precipitate. In contrast, the cesium chloride solution (beaker in the middle) did not show any signs of precipitation.

The resulting cesium chloride and sulfate solution was heated after centrifugation. However, as sulfuric acid has a boiling point of 337 °C, it did not volatilize completely at temperatures allowed for the used beaker. (Due to a lack of appropriate laboratory equipment, further evaporation has not been tested yet.) Another possibility to remove the acid in the solution, would be the addition of copper or lead to bind the ions belonging to the acid. This procedure would leave copper sulfate and lead

A.1. Precipitation of barium sulfate

sulfate in the solution, respectively. Therefore copper sulfate (CuSO_4) was tested as a matrix by dissolving CuSO_4 along with Cs_2SO_4 and subsequent boiling down ($\approx 100^\circ\text{C}$, decomposition of CuSO_4 at 560°C). The average atomic ratio measured on this targets was $\text{Ba}^{135}/\text{Cs}^{133} = (2.12 \pm 0.06) \times 10^{-8}$.

Bibliography

- Aoyama, M. and Hirose, K. (2008). Radiometric determination of anthropogenic radionuclides in seawater. In Pavel P. Povinec, editor, *Analysis of Environmental Radionuclides*, volume 11 of *Radioactivity in the Environment*, pages 137 – 162. Elsevier.
- Betz, H. D. (1972). Charge States and Charge-Changing Cross Sections of Fast Heavy Ions Penetrating Through Gaseous and Solid Media. *Rev. Mod. Phys.*, 44:465–539.
- Browne, E. and Tuli, J. (2007). Nuclear Data Sheets for $A = 137$. *Nuclear Data Sheets*, 108(10):2173 – 2318.
- Buchriegler, J. (2013). Construction of a Multi-Anode Ionization Chamber for AMS at VERA. *Master Thesis, University of Vienna*.
- Currie, L. A. (1968). Limits for qualitative detection and quantitative determination. Application to radiochemistry. *Analytical Chemistry*, 40(3):586–593.
- Dellinger, F., Forstner, O., Golser, R., Priller, A., Steier, P., Wallner, A., Winkler, G., and Kutschera, W. (2011). Ultrasensitive search for long-lived superheavy nuclides in the mass range $A=288$ to $A=300$ in natural Pt, Pb, and Bi. *Phys. Rev. C*, 83.
- Delmore, J. E., Snyder, D. C., Tranter, T., and Mann, N. R. (2011). Cesium isotope ratios as indicators of nuclear power plant operations. *Journal of Environmental Radioactivity*, 102(11):1008 – 1011.
- Dinev, D. (2009). Process in high energy heavy ion acceleration. *Physics of Particles and Nuclei*, 40(2):257–277.
- Eliades, J., Zhao, X.-L., Litherland, A., and Kieser, W. (2013). On-line ion chemistry for the AMS analysis of ^{90}Sr and $^{135,137}\text{Cs}$. *Nuclear Instruments and Methods in Physics Research Section B: Beam Interactions with Materials and Atoms*, 294:361 – 363.
- England, T. and Rider, B. (1993). Evaluation and compilation of fission product yields. *Los Alamos National Laboratory*.

Bibliography

- Forstner, O., Andersson, P., Diehl, C., Golser, R., Hanstorp, D., Kutschera, W., Lindahl, A., Priller, A., Steier, P., and Wallner, A. (2008). Isobar suppression in AMS using laser photodetachment. *Nuclear Instruments and Methods in Physics Research Section B: Beam Interactions with Materials and Atoms*, 266(19–20):4565 – 4568.
- Forstner, O., Andersson, P., Hanstorp, D., Lahner, J., Martschini, M., Pitters, J., Priller, A., Steier, P., and Golser, R. (2015). The ILIAS project for selective isobar suppression by laser photodetachment. *Nuclear Instruments and Methods in Physics Research Section B: Beam Interactions with Materials and Atoms*. In press.
- G Ryding and A B Wittkower and P H Rose (1969). Equilibrium Charge-State Distributions for Iodine in Gases (1-12 MeV). *Phys. Rev.*, 185:129–134.
- Granet, M., Nonell, A., Favre, G., Chartier, F., Isnard, H., Moureau, J., Caussignac, C., and Tran, B. (2008). Cs–Ba separation using N₂O as a reactant gas in a Multiple Collector-Inductively Coupled Plasma Mass Spectrometer collision-reaction cell: Application to the measurements of Cs isotopes in spent nuclear fuel samples. *Spectrochimica Acta Part B: Atomic Spectroscopy*, 63(11):1309 – 1314.
- Hou, X. and Roos, P. (2008). Critical comparison of radiometric and mass spectrometric methods for the determination of radionuclides in environmental, biological and nuclear waste samples. *Analytica Chimica Acta*, 608(2):105 – 139.
- Kaiser, H., Heinicke, E., Baumann, H., and Bethge, K. (1971). Molecular and atomic ions of the elements of the sub-groups of the periodic system. *Zeitschrift für Physik*, 243(1):46–59.
- Knoll, G. F. (1989). *Radiation detection and measurement; 2th ed.* Wiley, New York, NY.
- Kutschera, W., Collon, P., Friedmann, H., Golser, R., Hille, P., Priller, A., Rom, W., Steier, P., Tagesen, S., Wallner, A., Wild, E., and Winkler, G. (1997). VERA: A new AMS facility in Vienna. *Nuclear Instruments and Methods in Physics Research Section B: Beam Interactions with Materials and Atoms*, 123(1–4):47 – 50.
- Lachner, J., Kasberger, M., Martschini, M., Priller, A., Steier, P., and Golser, R. (2015). Developments towards detection of ¹³⁵Cs at VERA. *Nuclear Instruments and Methods in Physics Research Section B: Beam Interactions with Materials and Atoms*. In press.
- Lee, T., Teh-Lung, K., Hsiao-Ling, L., and Ju-Chin, C. (1993). First detection of fallout Cs-135 and potential applications of ¹³⁷Cs/¹³⁵Cs ratios. *Geochimica et Cosmochimica Acta*, 57(14):3493 – 3497.

- Mabit, L., Meusburger, K., Fulajtar, E., and Alewell, C. (2013). The usefulness of ^{137}Cs as a tracer for soil erosion assessment: A critical reply to Parsons and Foster (2011). *Earth-Science Reviews*, 127:300 – 307.
- MacDonald, C., Charles, C. R. J., Cornett, R. J., Zhao, X. L., Kieser, W. E., and Litherland, A. E. (2015). Detection of ^{135}Cs by accelerator mass spectrometry. *Rapid Communications in Mass Spectrometry*, 29(1):115–118.
- Martschini, M., Andersson, P., Forstner, O., Golser, R., Hanstorp, D., Lindahl, A. O., Kutschera, W., Pavetich, S., Priller, A., Rohlén, J., Steier, P., Suter, M., and Wallner, A. (2013). AMS of ^{36}Cl with the VERA 3 MV tandem accelerator. *Nuclear Instruments and Methods in Physics Research Section B: Beam Interactions with Materials and Atoms*, 294:115 – 120.
- Martschini, M., Buchriegler, J., Collon, P., Kutschera, W., Lachner, J., Lu, W., Priller, A., Steier, P., and Golser, R. (2015). Isobar separation of ^{93}Zr and ^{93}Nb at 24 MeV with a new multi-anode ionization chamber. *Nuclear Instruments and Methods in Physics Research Section B: Beam Interactions with Materials and Atoms*. *In press*.
- Middleton, R. (1983). A versatile high intensity negative ion source. *Nuclear Instruments and Methods in Physics Research*, 214(2–3):139 – 150.
- Middleton, R. (1989). A Negative-Ion Cookbook. *Department Of Physics, University of Pennsylvania, Philadelphia, PA 19104*.
- Milota, P., Reiche, I., Duval, A., Forstner, O., Guicharnaud, H., Kutschera, W., Merchel, S., Priller, A., Schreiner, M., Steier, P., Thobois, E., Wallner, A., Wünschek, B., and Golser, R. (2008). PIXE measurements of Renaissance silverpoint drawings at VERA. *Nuclear Instruments and Methods in Physics Research Section B: Beam Interactions with Materials and Atoms*, 266(10):2279 – 2285.
- Niklaus, T., Bonani, G., Guo, Z., Suter, M., and Synal, H.-A. (1994). Optimising tandem accelerator stripping efficiency by simulation of charge changing processes. *Nuclear Instruments and Methods in Physics Research Section B: Beam Interactions with Materials and Atoms*, 92(1–4):115 – 121.
- Parsons, A. and Foster, I. (2011). What can we learn about soil erosion from the use of ^{137}Cs ? *Earth-Science Reviews*, 108(1–2):101 – 113.
- Petrinin, V. V., Voldstad, J. D., Balling, P., Kristensen, P., Andersen, T., and Haugen, H. K. (1995). Resonant Ionization Spectroscopy of Ba^- : Metastable and Stable Ions. *Phys. Rev. Lett.*, 75:1911–1914.
- Pibida, L., Nörtershäuser, W., Hutchinson, J., and Bushawler, B. (2001). Evaluation of resonance ionization mass spectrometry for the determination of $^{135}\text{Cs}/^{137}\text{Cs}$ isotope ratios in low-level samples. *Radiochim. Acta*, 89:161–168.

Bibliography

- Priller, A., Melber, K., Forstner, O., Golser, R., Kutschera, W., Steier, P., and Wallner, A. (2010). The new injection beamline at VERA. *Nuclear Instruments and Methods in Physics Research Section B: Beam Interactions with Materials and Atoms*, 268(7–8):824 – 826.
- Rienstra-Kiracofe, J. C., Tschumper, G. S., Schaefer, H. F., Nandi, S., and Ellison, G. B. (2002). Atomic and Molecular Electron Affinities: Photoelectron Experiments and Theoretical Computations. *Chemical Reviews*, 102(1):231–282.
- Sayer, R. (1977). Semi-empirical formulas for heavy-ion stripping data. *Revue de Physique Appliquee*, 12(10):1543–1546.
- Schmidt, E. (2013). AMS detection of ^{10}Be with a SiN-foil stack. *Master Thesis, University of Vienna*.
- Singh, B., Rodionov, A. A., and Khazov, Y. L. (2008). Nuclear Data Sheets for $A = 135$. *Nuclear Data Sheets*, 109(3):517 – 698.
- Srncik, M., Wallner, G., Hrnccek, E., Steier, P., Wallner, A., and Bossew, P. (2008). Vertical distribution of ^{238}Pu , $^{239}(40)\text{Pu}$, ^{241}Am , ^{90}Sr and ^{137}Cs in Austrian soil profiles. *Radiochimica Acta*, 96:733–738.
- Steier, P. (2000). Exploring the limits of VERA: A universal facility for accelerator mass spectrometry. *PhD Thesis, University of Vienna*.
- Steier, P., Dellinger, F., Forstner, O., Golser, R., Knie, K., Kutschera, W., Priller, A., Quinto, F., Srncik, M., Terrasi, F., Vockenhuber, C., Wallner, A., Wallner, G., and Wild, E. M. (2010). Analysis and application of heavy isotopes in the environment. *Nuclear Instruments and Methods in Physics Research Section B: Beam Interactions with Materials and Atoms*, 268(7–8):1045 – 1049.
- Steier, P., Golser, R., Kutschera, W., Priller, A., Vockenhuber, C., and Winkler, S. (2004). VERA, an AMS facility for “all” isotopes. *Nuclear Instruments and Methods in Physics Research Section B: Beam Interactions with Materials and Atoms*, 223–224:67 – 71.
- Taylor, V., Evans, R., and Cornett, R. (2008). Preliminary evaluation of $^{135}\text{Cs}/^{137}\text{Cs}$ as a forensic tool for identifying source of radioactive contamination. *Journal of Environmental Radioactivity*, 99(1):109 – 118.
- Vockenhuber, C., Ahmad, I., Golser, R., Kutschera, W., Liechtenstein, V., Priller, A., Steier, P., and Winkler, S. (2003). Accelerator mass spectrometry of heavy long-lived radionuclides. *International Journal of Mass Spectrometry*, 223–224:713 – 732.

Acknowledgments

First of all, I want to thank Robin Golser for giving me the opportunity to write my diploma thesis at VERA and being my supervisor — despite his busy schedule, he found time for discussions and many valuable suggestions. I also feel very lucky for the co-supervision of Johannes Lachner, who patiently answered my questions and never lacked of great ideas, which he generously shared with me.

I thank the whole VERA staff for providing such a nice atmosphere at the institute, especially: Alfred Priller for being most patient in all technical troubles with “haudigem Klump“. Martin Martschini for sharing his knowledge and help in the measurements with MAIC. Peter Steier for seemingly knowing everything about the accelerator. Helga Schmelzer-Vincro and Sigrid Lielacher for thinking of everything and always being willing to help. The staff of the workshop Ewald Friedl, Gabi Obstmayer and Johann Lukas for helping out with their mechanical skills and computer support along with a friendly smile. Monika Bolka for teaching me basics in the proper treatment of lab equipment and for the nice hallway-conversations.

I thank “the girls“ Jenny Feige and Johanna Pitters for keeping me healthy during my time at VERA, with vitamins, sport and lots of laughter. Thank you, Marco Ploner, for convincing me to write this thesis in the first place and being such a pleasant office colleague. I am also very grateful for the amusing times at lunch with Tobias Moreau and our “seniors“ Johannes Lachner and Martin Martschini, who never got tired of encouraging and helping us with our work. I enjoyed being here from the first day on! Furthermore, I want to express my gratitude to all the proofreaders for investing their time and being both, kind and thorough.

I think back on my studies with satisfaction for spending many joyful hours with my colleagues Claudia Zimmermann, Emma Kolb, Erich Zöchmann, Florian Reischl, Katharina Gaal, Markus Meiringer, Martin Nikodim, Patrick Ritt, Reingard Auer and Valentin Parzer — Thank you!

Ich danke meiner Familie für ihre stets offenen Ohren und das Interesse an meinem Studium. Mein ganz besonderer Dank gebührt dabei meinen Eltern, Wilma und Erwin, die mir dieses Studium mit der größten Selbstverständlichkeit ermöglicht haben und sich die Fragen nach einem baldigen Studienende auch bis fast ganz zum Schluss aufsparten! Meinem Mann Johannes danke ich für die tatkräftige Unterstützung mit seinen Programmierkenntnissen und für die Geduld, die er mit mir hatte.

Curriculum Vitae

Personal

Name Magdalena Katharina Kasberger
E-Mail a0905670@unet.univie.ac.at

Education

1997-2001	Elementary School in Oftring, Austria
2001-2009	Secondary School, WRG der Franziskanerinnen in Wels, Austria
June 2009	Graduation (Matura)
since 2009	Diploma study in Physics and Mathematics (teacher's curriculum), University of Vienna
since July 2014	Diploma Thesis at the VERA Laboratory, Faculty of Physics, University of Vienna (supervisor: Prof. Robin Golser): <i>Accelerator Mass Spectrometry of Cesium Isotopes</i>

Publications

- Johannes Lachner, Magdalena Kasberger, Martin Martschini, Alfred Priller, Peter Steier, Robin Golser, Developments towards detection of ^{135}Cs at VERA, Nucl. Instrum. Meth. B (2015). In press.